

TOPICAL REVIEW • OPEN ACCESS

GaAs-based micro/nanomechanical resonators

To cite this article: Hiroshi Yamaguchi 2017 *Semicond. Sci. Technol.* **32** 103003

View the [article online](#) for updates and enhancements.

You may also like

- [Dynamics of 2D material membranes](#)
Peter G Steeneken, Robin J Dolleman,
Dejan Davidovikj et al.
- [Design of black phosphorus 2D
nanomechanical resonators by exploiting
the intrinsic mechanical anisotropy](#)
Zenghui Wang and Philip X-L Feng
- [2D-materials-integrated
optoelectromechanics: recent progress
and future perspectives](#)
Mingzeng Peng, Jiadong Cheng, Xinhe
Zheng et al.



ECS
The
Electrochemical
Society
Advancing solid state &
electrochemical science & technology

DISCOVER
how sustainability
intersects with
electrochemistry & solid
state science research

Topical Review

GaAs-based micro/nanomechanical resonators

Hiroshi Yamaguchi

NTT Basic Research Laboratories, Nippon Telegraph and Telephone Corporation, 3-1, Morinosato-Wakamiya, Atsugi-shi, Kanagawa, 243-1098 Japan

E-mail: yamaguchi.hiroshi@lab.ntt.co.jp

Received 5 October 2015, revised 2 August 2017

Accepted for publication 10 August 2017

Published 11 September 2017



CrossMark

Abstract

Micro/nanomechanical resonators have been extensively studied both for device applications, such as high-performance sensors and high-frequency devices, and for fundamental science, such as quantum physics in macroscopic objects. The advantages of GaAs-based semiconductor heterostructures include improved mechanical properties through strain engineering, highly controllable piezoelectric transduction, carrier-mediated optomechanical coupling, and hybridization with quantum low-dimensional structures. This article reviews our recent activities, as well as those of other groups, on the physics and applications of mechanical resonators fabricated using GaAs-based heterostructures.

Keywords: MEMS, NEMS, mechanical resonators, phonon, nonlinear dynamics

(Some figures may appear in colour only in the online journal)

1. Introduction

Mechanical resonators are three-dimensional structures that implement the dynamics of harmonic oscillators. They have traditionally been used in many apparatuses, such as pendulum clocks and musical instruments. Recent advances in microfabrication technology have made it possible to fabricate ultra-small mechanical resonators. This has led to the development of a new category of devices called micro or nanomechanical resonators [1–4], which are now used in practical, commercially available devices such as cantilevers for scanning probe microscopes and microwave filters as well as the oscillators for mobile phone applications [5, 6].

Owing to these technological developments, a new field of science has emerged to explore the fundamental physics of minute mechanical resonators. Micro/nanomechanical resonators are advantageous in these studies for their high-

frequency operation and sharp resonance characteristics. The resonance frequency of their fundamental mode ($f_0 \equiv \omega_0/2\pi$) reaches the gigahertz range [7–13], and the quality factor (Q) exceeds one million [14–17] although these two performances have not yet been simultaneously demonstrated. Because of these excellent resonance characteristics, mechanical resonators in the quantum regime have become a highly focused target of research in fundamental physics [18–22]. When the thermal energy becomes smaller than the energy quantum of a harmonic oscillator, the quantum ground state of a mechanical resonator is achieved. The condition at the base temperature of a dilution refrigerator (~ 50 mK) is $f_0 > 1$ GHz, which can be satisfied using submicron-long beam resonators.

Micro/nanomechanical resonators exhibit significant nonlinear dynamics [3, 23, 24]. A doubly clamped beam resonator naturally shows the mechanical nonlinearity induced by oscillation-induced beam tension. For a single-mode system, the nonlinearity leads to bi-stable oscillation, which is applicable to mechanical memory [25–32] and bifurcation detectors [33]. The nonlinearity in a multi-mode system causes their intermodal coupling [34–41]. The



Original content from this work may be used under the terms of the [Creative Commons Attribution 3.0 licence](https://creativecommons.org/licenses/by/3.0/). Any further distribution of this work must maintain attribution to the author(s) and the title of the work, journal citation and DOI.

difference or sum of two mode frequencies applied as the periodic parametric modulation results in frequency conversion [42], two-mode squeezing [43], and phonon lasing operation [44].

High-Q mechanical resonators are practically important in applications to physical sensors [45, 46]. Owing to their extreme sensitivity to external forces, they have been used not only in practical devices, such as high-performance biomolecular [47] and magnetic sensors [48] but also in the study of fundamental science. For the latter, they serve as ‘probes’ of microscopic phenomena emerging in nanoscale structures, such as quantum low-dimensional structures and spintronic systems. As a technique that complements the conventional electric and optical characterization, the mechanical probe can be used to investigate different profiles of microscopic phenomena. Examples using semiconductor quantum structures will be briefly introduced in section 5.

For fabricating mechanical resonators, compound semiconductors have several advantages over other material systems. One is that high-quality and single-crystalline multilayer heterostructures can be formed by using state-of-the-art crystal growth techniques like molecular beam epitaxy (MBE) and metal organic vapor phase epitaxy (MOVPE). The film uniformity is on the order of monolayer thickness, and high-performance mechanical structures can be easily fabricated using standard micro/nanofabrication techniques. In addition, the film strain control by using strained layer heterostructures enables the fabrication of novel nanostructures [49–51] and can drastically improve the resonance characteristics as well [52, 53].

Another advantage is integration with optical and electronic devices. Compound semiconductors are commonly used to fabricate optical devices, such as semiconductor lasers and detectors, and electronic ones, such as high-mobility transistors and resonant tunneling diodes. Their hybrid devices allow novel application such as mechanically controlled semiconductor lasers [54] and on-chip amplified force sensors [55, 56].

A third is piezoelectricity, which can be utilized for high-performance stress/strain-voltage transduction. As shown in section 2.3, ideal electrical control of parametric resonators has been demonstrated using piezoelectric strain-voltage transduction [27, 57–60]. The piezoelectricity can also be utilized for transduction between optical signal and mechanical motion, which is important in carrier-mediated optomechanical systems [61–63].

Last but not least is integration with quantum low-dimensional structures. Mechanical resonators can be coupled to quantum structures through strain effects, i.e., piezoelectricity and deformation potential. The quantum mechanical properties of photons, carriers, and spins can be mechanically characterized and controlled through the strain-mediated coupling.

In this article, studies using GaAs-based micro/nano-mechanical resonators are overviewed. This review paper is organized as follows. The next section describes fundamentals of GaAs-based mechanical resonators, including their resonance characteristics, fabrication processes, and the

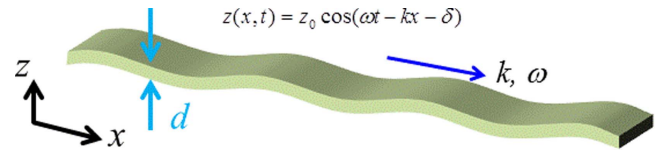


Figure 1. Schematic drawing of an infinitely long beam with thickness d . The travelling-wave solution is given by equation (2) with the dispersion relation (3).

piezoelectric properties. Section 3 details the application of GaAs/AlGaAs heterostructures to electromechanical parametric resonators. The fundamental theory and experimental demonstrations are both examined in detail. Section 4 describes the carrier-mediated optomechanical properties. In a way similar to cavity optomechanics, laser cooling and amplification of thermal motion are both demonstrated through the back action force induced by the generated electron-hole pairs, i.e., excitations. Section 5 covers the hybridization with quantum low-dimensional electron systems. The interaction of mechanical motion with a two-dimensional (2D) electron system in the quantum Hall regime as well as with a zero-dimensional (0D) electron system in a quantum dot (QD) is described.

2. Fundamental properties of GaAs-based cantilevers and beam resonators

2.1. Eigenfrequency and eigenfunction of beam resonators

In this section, we describe the dynamics of mechanical resonators using a standard theory for suspended structures. The flexural motion of a suspended one-dimensional (1D) beam structure is described by the Euler–Bernoulli equation [1, 3, 64]

$$\frac{Ed^2}{12} \frac{\partial^4 z(x, t)}{\partial x^4} + \rho \frac{\partial^2 z(x, t)}{\partial t^2} = 0, \quad (1)$$

where $z(x, t)$ is the displacement of the beam at longitudinal position x and time t , E is the Young’s modulus, d is beam thickness, and ρ is density. For an infinitely long beam (figure 1), the equation has the following solution of freely propagating waves:

$$z(x, t) = z_0 \cos(\omega t - kx - \delta) \quad (2)$$

$$\omega = k^2 d \sqrt{E/12\rho}, \quad (3)$$

Here, δ is the phase factor, k is the wavenumber, ω is the angular frequency, and z_0 is the arbitral real number amplitude. Equation (3) gives the dispersion relation of an elastic transverse wave propagating through this infinitely long 1D beam.

For a mechanical resonator, a boundary condition applied at the edge of the beam leads to the discrete eigenfrequency. Doubly clamped and cantilever beams are two typical mechanical resonators (figure 2). Hereafter, we simply refer to them as a beam and a cantilever, respectively.

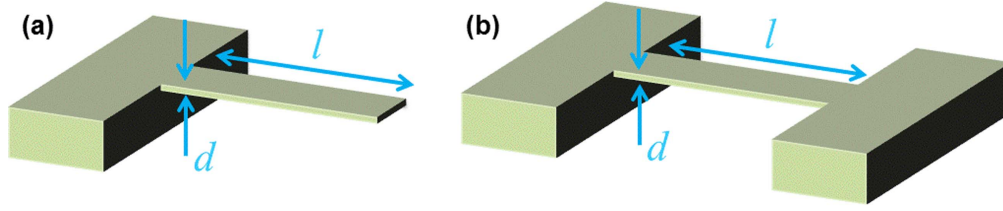


Figure 2. Schematic drawings of (a) a cantilever beam and (b) a doubly clamped beam with length l and thickness d . In the 1D Euler–Bernoulli beam theory, the resonance frequency does not depend on the beam width, which is assumed to be sufficiently larger than the thickness.

Table 1. Calculated fundamental resonance frequencies of GaAs beams and cantilevers with aspect ratio $l/d = 20$.

Length (l)	100 μm	3 μm	100 nm
$\omega_1/2\pi$ (beam)	2.06 MHz	68.7 MHz	2.06 GHz
$\hbar\omega_1/k_B$ (beam)	99 μK	3.3 mK	99 mK
$\omega_1/2\pi$ (cantilever)	0.32 MHz	10.8 MHz	0.32 GHz
$\hbar\omega_1/k_B$ (cantilever)	15.5 μK	0.52 mK	15.5 mK

The conditions for a beam and cantilever with length l are given by

$$z(0, t) = z'(0, t) = z(l, t) = z'(l, t) = 0 \quad (\text{beam}). \quad (4)$$

$$z(0, t) = z'(0, t) = z''(l, t) = z'''(l, t) = 0 \quad (\text{cantilever}). \quad (5)$$

Here, the prime means the derivative with respect to the coordinate variable x . Condition (5) is satisfied because no force and bending moment are applied at the unclamped edge [1, 3]. The m th eigenfunction (i.e., the waveform of the vibrational mode) $u_m(x)$ and eigenwavenumber k_m are then given by

$$u_m(x) = A_m \sin(k_m x) + B_m \cos(k_m x) + C_m \sinh(k_m x) + D_m \cosh(k_m x), \quad (6)$$

$$k_m = \lambda_m / l$$

$$\lambda_1 = 4.730, \lambda_2 = 7.853, \lambda_3 = 10.996, \dots (\text{beam}).$$

$$\lambda_1 = 1.875, \lambda_2 = 4.712, \lambda_3 = 7.854, \dots (\text{cantilever}). \quad (7)$$

The ratios of coefficients $A_m \sim D_m$ are also determined by the boundary condition [1, 3]. The m th eigenfrequency f_m is then given by

$$f_m \equiv \frac{\omega_m}{2\pi} = \frac{\lambda_m^2 d}{2\pi l^2} \sqrt{\frac{E}{12\rho}}. \quad (8)$$

Equation (7) shows that the fundamental ($m = 1$) eigenfrequency of a beam is higher than a cantilever's by more than a factor of 6. It is proportional to beam thickness d while inversely proportional to the length squared l^2 , so that the frequency linearly increases with uniformly decreasing the structure size. The calculated fundamental eigenfrequencies are shown for GaAs in table 1. The frequency can be in the gigahertz range for submicrometer-long beam structures [18].

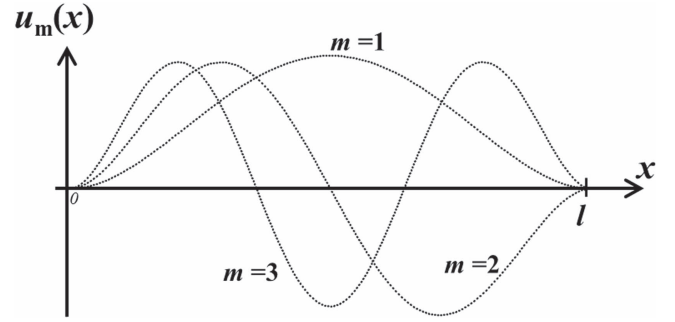


Figure 3. Calculated lowest three mode functions for a beam resonator.

The m th mode eigenfunction $u_m(x)$ satisfies boundary conditions (4) or (5) and the eigenequation

$$\frac{d^4 u_m(x)}{dx^4} = \frac{12\rho\omega_m^2}{Ed^2} u_m(x). \quad (9)$$

We can choose dimensionless eigenfunctions $u_m(x)$ that satisfy the orthonormal condition.

$$\int_0^l u_m(x) u_n(x) dx / l = \delta_{mn} \quad (10)$$

Figure 3 shows the first three vibrational mode shapes, u_1 , u_2 , and u_3 , of a beam resonator. We can expand general waveform $z(x, t)$ using these eigenfunctions as

$$z(x, t) = \sum_{m=1}^{\infty} q_m(t) u_m(x) \quad (11)$$

Using orthonormal condition (10), equation (1) leads to the equation of motion for a harmonic oscillator with mode displacement $q_m(t)$:

$$\ddot{q}_m(t) = -\omega_m^2 q_m(t) \quad (12)$$

Here, the over-dot is used for the derivative with respect to time t . The beam resonator can be regarded as an ensemble of independent (non-interacting) harmonic oscillators. This result is altered when the effect of beam tension is taken into account, where the orthogonal normal modes are mixed by external or vibration-induced tension. This is an important property for describing the nonlinearity and mode-mode coupling as shown in section 3.

In real systems, the equation of motion is modified by taking into account the effect of energy dissipation. When the system has damping rate $\gamma_m \equiv \omega_m / Q_m$ (where Q_m is the mode

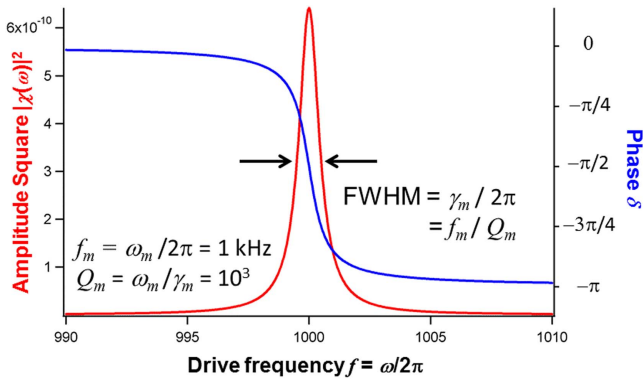


Figure 4. Calculated $|\chi_m(\omega)|^2$, which is proportional to the amplitude squared and the vibration energy, and phase δ as a function of drive frequency. The ratio of the resonance frequency to the FWHM gives the quality factor Q_m .

quality factor) and is driven by external force $F_m(t) \equiv mf_m(t)$ with beam mass $m \equiv \rho lwd$ (where w is the beam width), the equation of motion becomes

$$\ddot{q}_m(t) = -\gamma_m \dot{q}_m(t) - \omega_m^2 q_m(t) + f_m(t). \quad (13)$$

The solution for periodic force $f_m(t) = g_0 \cos(\omega t)$ can be easily obtained as

$$q_m(t) = |\chi_m(\omega)| g_0 \cos(\omega t + \delta), \quad \delta = \arg \chi_m(\omega), \quad (14)$$

where $\chi_m(\omega)$ is the mechanical susceptibility defined as

$$\chi_m(\omega) \equiv 1/(\omega_m^2 - \omega^2 + i\gamma_m\omega). \quad (15)$$

The vibration amplitude squared $g_0^2 |\chi_m(\omega)|^2$, which is proportional to the vibration energy, shows the well-known Lorentzian frequency dependence with the center frequency of $\omega_m/2\pi$ and the full width at half maximum (FWHM) of $\gamma_m/2\pi = \omega_m/2\pi Q_m$ as shown in figure 4.

2.2. Structure fabrication

GaAs-based mechanical resonators are fabricated by utilizing standard micromachining techniques with selective etching. Thin-film crystal growth methods, such as MBE and MOVPE, are used to prepare the layer structures, where a micrometer-thick sacrificial layer is grown under the ‘resonator’ layer. After the lateral structures have been defined with the electrodes prepared, the sacrificial layer is selectively etched to release the structure from the substrate (figure 5). As mentioned in section 1, one of the largest advantages of using compound semiconductor as the host material of micro/nanomechanical structures is hybridization with electronic and optical devices. The selective etching can be easily performed to release the mechanical structures that are also integrated with these devices. Examples of hybrid structures are shown in figure 6.

For the GaAs/AlGaAs system, a high-Al-composition ($x > 0.6$) $\text{Al}_x\text{Ga}_{1-x}\text{As}$ layer is used as the sacrificial layer. A solution of hydrofluoric (HF) acid has high etching selectivity for releasing the mechanical structures [27, 54]. To avoid degradation due to the HF etching, chromium gold (CrAu) is employed for the deposition of Schottky contacts. The

sacrificial layer etching for other III-V compound semiconductors includes XeF_2 dry etching for GaN/AlGaAs on Si substrates [59, 71], wet etching using sulfuric acid [72] and HF [73] for InP-based structures, and ammonia wet etching for InAs/AlGaSb on GaAs substrate [66, 74, 75].

As mentioned in section 1, the epitaxial tension can greatly improve the mechanical resonance characteristics [52, 53, 76, 77]. The improvement was first demonstrated using CVD-grown amorphous SiN films [76]. The concept was applied to single crystalline compound semiconductor systems: GaAs/In(Al)GaAs [52], GaNAs/GaAs [53], and InGaP/GaAs [77]. In all cases, the tension applied to the beam via the epitaxial strain increased the resonance frequency. Furthermore, the Q factor becomes orders of magnitude higher than for unstrained film.

The bottom-up process of semiconductor nanostructures is also employed for fabricating mechanical resonators, and semiconductor nanowires are especially promising nanostructures [78–85]. In contrast to the optical motion detection [79–85], a precise nanowire alignment process is needed in the fabrication of nanowire electromechanical devices [78, 83], where the motion can be electrically detected.

2.3. Piezoelectric transduction and measurement setup.

The piezoelectricity of compound semiconductors is also advantageous in these material systems. Not only electromechanical but also optomechanical transduction becomes possible through piezoelectricity with the very high crystalline quality of mechanical structures maintained. It is well known that the uniaxial piezoelectricity is maximized along the (111) axis in zinc blend crystal structures, so that a layer grown on (111)-oriented substrate is useful for conventional devices such as bulk acoustic resonators [86, 87]. However, the piezoelectric transduction between two orthogonal directions, [001] and [110], can be accessed for layer structures grown on (001) substrate through the d_{31} piezoelectric component [27, 57]. Figure 7 schematically shows the typical piezoelectric voltage-stress transduction in GaAs. By preparing two parallel-plate electrodes and applying a voltage in the surface normal direction, stress along the [110] direction is generated. Because the GaAs and AlGaAs are elastically and piezoelectrically isotropic materials, stress can be generated also in the $[-110]$ direction with the opposite polarity. This transduction scheme can be applied to fabricate GaAs/AlGaAs piezoelectric mechanical resonators as shown in figure 8. Surface and back-surface electrodes are formed by a top Schottky metal layer and a Si-doped conductive n-GaAs layer, respectively. To enhance their insulation, a layer of $\text{Al}_x\text{Ga}_{1-x}\text{As}$ is sandwiched between them, where the composition ratio x is kept lower than 0.3 to avoid damage by the following HF etching.

The voltage-induced piezoelectric stress generates a bending moment in the beam structures, leading to the actuation of flexural motion. The reversed transduction, i.e., the generation of motion-induced piezovoltage, is measured between the two electrodes, allowing the electrical detection of the mechanical motion. In addition, applying a voltage

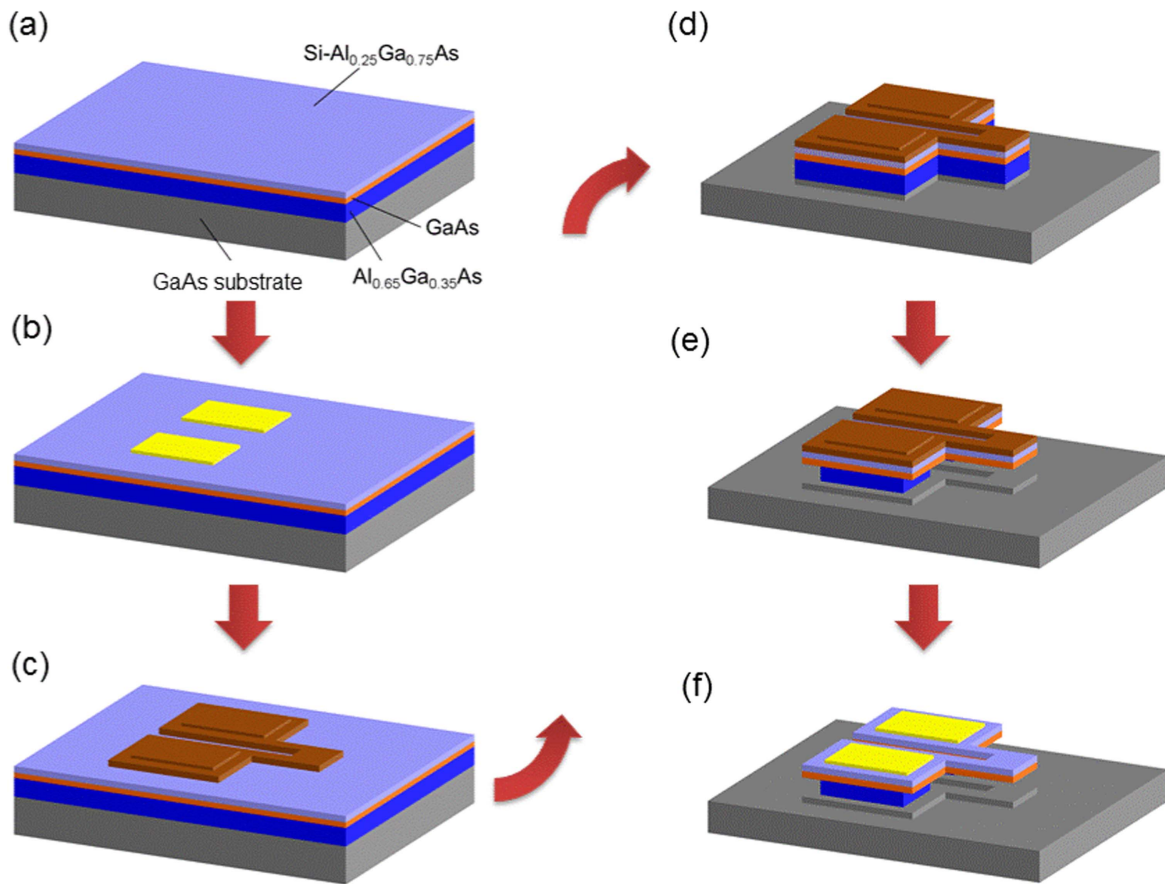


Figure 5. Fabrication process for a GaAs/AlGaAs piezoresistive cantilever used in [63]. (a) The electromechanically active structure of Si-doped $\text{Al}_{0.25}\text{Ga}_{0.75}\text{As}$ (light blue) and GaAs (orange) modulation-doped heterostructure are grown on the sacrificial layer of $\text{Al}_{0.65}\text{Ga}_{0.35}\text{As}$ (dark blue). (b) AuGeNi Ohmic contact electrodes (yellow) are deposited, followed by the metallization annealing process. (c) The cantilever-shaped resist pattern (brown) is defined by photolithography. (d) Wet or dry etching is performed down to the sacrificial layer. (e) The sacrificial layer is selectively etched using a solution of hydrofluoric acid to release the cantilever. (f) Finally, the resist pattern is removed. The cantilever vibration is electrically measurable as the resistance change between two Ohmic electrodes [63].

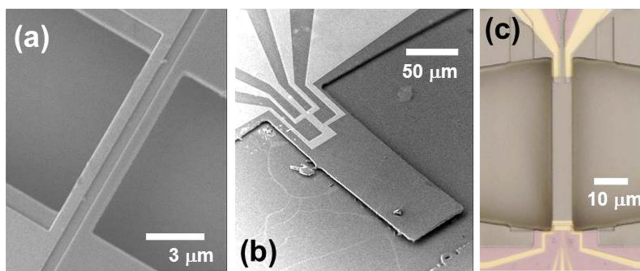


Figure 6. Examples of fabricated semiconductor electromechanical resonators integrated with quantum low-dimensional structures. (a) Quasi-one-dimensional InAs channel [66], (b) high mobility 2D GaAs/AlGaAs heterostructure Hall bar [67, 68] (Copyright 2007 The Japan Society of Applied Physics), and (c) GaAs/AlGaAs QD [69, 70] (reprinted from Appl. Phys. Lett. 103, 192105 with the permission of AIP Publishing).

between the electrodes induces beam tension and modifies the resonance frequency. This third function is important for applying this structure to parametric resonators [27] (the details will be quantitatively explained in the next section). Therefore, this simple structure has three fundamental functions: actuation, detection, and frequency tuning of mechanical resonance. Figure 9(b) shows an example of the

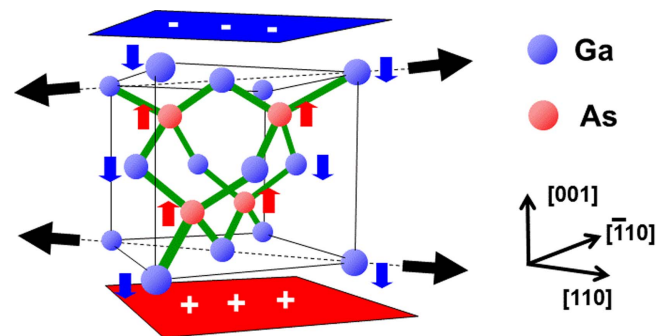


Figure 7. Schematic drawing of piezoelectric voltage-stress transduction. When the electric field is applied along the [001] direction, Ga and As atoms are forced downward and upward, respectively. Due to the diamond-like bond alignments in a zinc blende structure, the resultant stress is applied in the [110] direction.

resonance characteristics of a GaAs/AlGaAs beam resonator [figure 9(a)] as a function of gate voltage. The actuation and detection are both performed by using the piezoelectric transduction. The linear shift of the resonance frequency induced by the constant gate voltage is clearly confirmed.

The displacement sensitivity in this device is in the range of picometers even at cryogenic temperatures if we simply

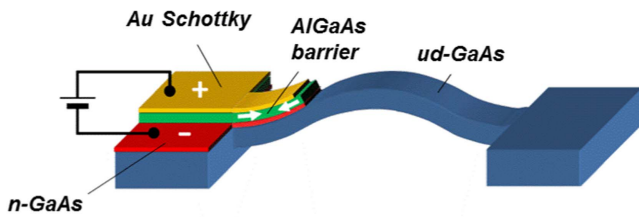


Figure 8. Schematic drawing of a GaAs/AlGaAs piezoelectric resonator. The piezoelectric AlGaAs barrier layer is sandwiched between the top Au Schottky gate and conductive n-GaAs layer. The voltage applied between them induces stress along the beam direction (white arrows). Because this stress is applied only on the near-surface region of a GaAs beam, it induces a bending moment to drive the flexural mechanical motion.

measure the generated piezovoltage with a commercial amplifier. This sensitivity can be improved by fabricating an on-chip amplifier. One example is given by integrating a field effect transistor into a mechanical resonator. The first report was by Beck *et al* in 1994 [89], followed by its cryogenic application [90]. Then a smaller structure with a displacement sensitivity of $9 \text{ pm Hz}^{-1/2}$ at room temperature was reported [91]. The integration of a semiconductor quantum point contact (QPC) or QD further enhances the sensitivity at cryogenic temperatures [69, 70, 92–94].

Laser interferometers are widely used to detect motion for various types of mechanical resonators. The sensitivity is generally higher than the piezoelectric transduction, although the detection in a cryogenic environment requires precisely aligned optical access. In some studies introduced in this review paper, an optical interferometer was also employed, especially for the detection of thermal motion.

In the field of cavity optomechanics, the coupling of mechanical resonators with an optical cavity greatly enhances the detection sensitivity. The scheme also allows parametric coupling between light and mechanical oscillation, which makes it possible to realize optomechanical cooling. This topic is out of the scope of this article, but comprehensive review articles have already been published [19, 95, 96]. Cavity optomechanics is also studied using GaAs-based mechanical resonators [12, 97–99].

3. Parametric electromechanical resonators

In this section, parametric electromechanical resonators—one of the most important applications of GaAs-based micro-mechanical resonators—are described in detail. A parametric resonator is a harmonic oscillator where the oscillations are driven by periodically modulating some parameter of the system, such as spring and coupling constants, at a different frequency from the resonator eigenfrequency. Parametric resonators have been demonstrated in many physical systems, from electronic circuits in radio and microwave frequencies to optical cavities and one of its most important applications is a very low noise amplifier. For example, it was used in a radio telescope used in Project Ozma started in 1960, and recently superconducting resonators are used for the parametric

amplifiers with quantum-limited performance [100]. As described in 3.3, parametric resonators can be utilized in many other purposes from quantum physics to signal processors, such as squeezed state generation and frequency conversion.

Similar functions of parametric resonators can be imported in mechanical domains. Mechanical parametric resonators have been constructed by utilizing several transduction schemes such as magnetic force gradient [101], electrostatic force [102–104], laser-induced thermal expansion [105], and dielectric dipole force [106]. The advantage of piezoelectric GaAs-based resonators is their built-in nature, which allows highly stable and efficient operation, as also reported with GaN-based material systems [107].

In parametric resonators, the resonance frequency (or any coefficient in the equations of motion in general [108]) is periodically modulated by external means. In GaAs/AlGaAs-based resonators, the frequency modulation is induced by piezoelectric stress generated by the applied voltage as described in the previous section. For example in the device shown in figure 9(a), the frequency can be periodically modulated by applying AC voltage on one of the gate electrodes. There are two operational modes of parametric resonators. One is ‘parametric amplification’, where an externally driven vibration, called a ‘signal’, is amplified by a ‘pump’, which is an externally applied periodic resonance frequency modulation at a frequency different from that of the signal. The other operation mode is parametric oscillation, where the gain of the parametric amplification becomes infinity and the self-sustained oscillation is activated without applying the signal. Parametric amplification can be also categorized into two types (figure 10). One is degenerate parametric amplification, where the pump has twice the signal frequency. In this case, the amplified vibration has the same frequency as the signal. The other is non-degenerate parametric amplification. In this case, a mechanical vibration with a different frequency from the signal, called an idler, is newly generated. Therefore non-degenerate parametric amplification has a frequency conversion function. In the following sections, the theoretical formulation for parametric resonators and the implementation by GaAs/AlGaAs parametric resonators are described in detail.

3.1. Tension-induced frequency modulation

First, the tension-induced frequency modulation is theoretically described in single-beam resonators [109, 110]. The Hamiltonian formalism is useful for that purpose because the effect of tension can be easily introduced as shown in appendix A. Using m th-mode displacement $q_m(t)$ defined in equation (11) and its conjugate momentum $p_m(t) = m\dot{q}_m(t)$ with total beam mass $m \equiv \rho l w d$ (where w is the beam width), the Hamiltonian is expressed as (see appendix A)

$$H_0 = \sum_m \left(\frac{p_m^2}{2m} + \frac{m\omega_m^2 q_m^2}{2} \right). \quad (16)$$

The system can be regarded as an ensemble of independent harmonic oscillators, as already mentioned in section 2. We

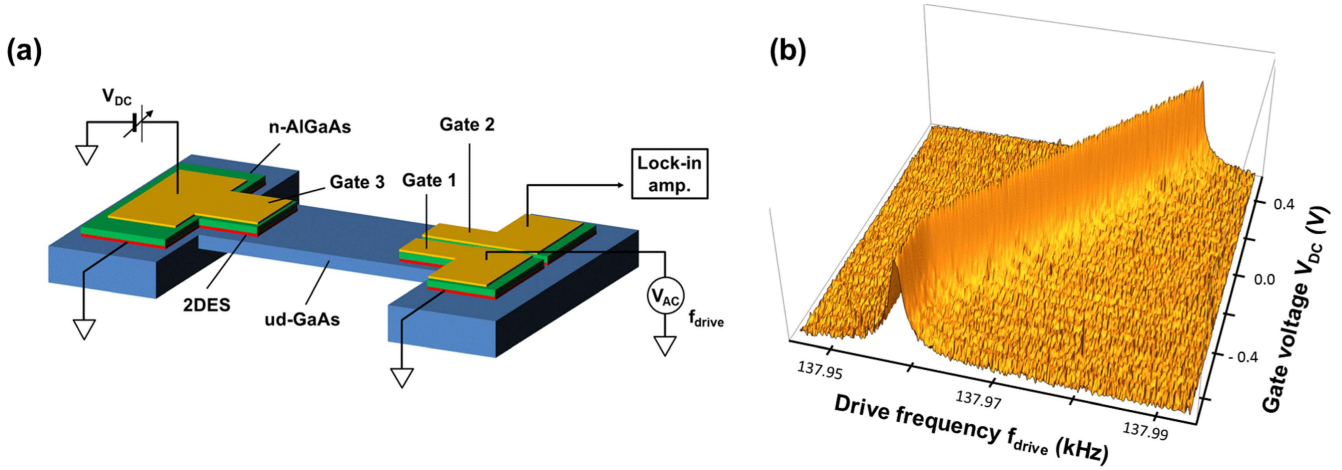


Figure 9. (a) Schematic drawing of a fabricated GaAs/AlGaAs piezoelectric resonator as well as the experimental setup for the measurement of resonance characteristics. Instead of the layer structure shown in figure 8, a modulation doped heterostructure composed of Si-doped n-AlGaAs (green) and undoped GaAs (blue) is used in this experiment. The piezoelectric transduction can be made using the top Au contact (yellow) and 2D electron system (2DES: red) as two parallel-plate electrodes. The AC voltage applied on Gate 1 drives the mechanical motion, which is detected through the voltage generated on Gate 2 measured by a lock-in amplifier. (b) Resonance characteristics measured as a function of the DC voltage (V_{DC}) applied to Gate 3. The z-axis shows the vibration amplitude. The linear shift in the resonance frequency induced by the piezoelectric tension is clearly confirmed [27]. Frequency saturation is observed with gate voltage lower than -0.4 V corresponding to the electron depletion in the conductive layer, showing that the piezoelectric strain between the gate and 2DES is responsible for the frequency shift. In contrast to the study reported in [88], we used separate gate electrodes for actuation and frequency modulation so that the mechanical oscillation can be induced even when the 2DES is fully depleted by Gate 3. The measurement was performed at 2.5 K in vacuum.

discuss here the case of doubly clamped beam resonators because the parametric nonlinear interaction can be naturally introduced by the beam tension. Tension τ is decomposed into two parts: externally applied tension and that induced by beam vibration. External tension $\tau_{ext}(t)$ can be electrically applied by piezoelectric effects in our GaAs/AlGaAs-based devices, as shown in the previous section. The tension is proportional to the applied voltage as $\tau_{ext}(t) = cV_g(t)$, where c is the piezoelectric coupling constant and $V_g(t)$ is the applied gate voltage, so that the tension can be precisely controlled by electrical means. If we take into account only the tension externally applied, the lowest order contribution is given by

$$H = H_0 + \frac{\tau_{ext}}{2l} \sum_{m,n} T_{mn} q_m(t) q_n(t). \quad (17)$$

When only the n th mode is taken into account, the Hamiltonian is given by

$$H_n = \frac{p_n^2}{2m} + \frac{(m\omega_n^2 + \tau_{ext} T_{nn}/l) q_n^2}{2}. \quad (18)$$

This equation shows that the resonance frequency is modified as

$$\omega_n \rightarrow \omega_n \sqrt{1 + \frac{\tau_{ext} T_{nn}}{lm\omega_n^2}} \sim \omega_n + \frac{T_{nn}}{2lm\omega_n} \tau_{ext} \quad (19)$$

by the applied tension. In GaAs-based parametric resonators, the gate voltage induces the tension, leading to the modulation of the resonance frequency. Equation (17) also shows that the external tension can induce linear coupling between different modes. For example, the Hamiltonian of modes n

and m is given by

$$H = \frac{p_n^2}{2m} + \frac{m\omega_n^2 q_n^2}{2} + \frac{p_m^2}{2m} + \frac{m\omega_m^2 q_m^2}{2} + \frac{\tau_{ext}}{2l} T_{nm} q_n q_m, \quad (20)$$

where the last term gives the intermodal coupling [111]. This Hamiltonian is important for describing intermodal parametric coupling, as shown in section 3.4. Intermodal coupling in other multimode systems has also been reported [112, 113]. The parametrically coupled two mode system can be similarly constructed using paired resonators as shown in appendix B.

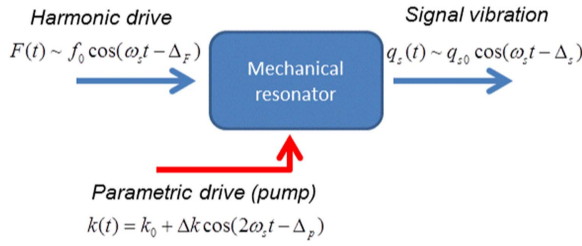
3.2. Degenerate parametric amplification and resonance

We then consider the case where the tension is periodically modulated at frequency ω_p , i.e., $\tau_{ext}(t) = \tau_0 \sin \omega_p t$. The periodic modulation is called the pump, being analogous to nonlinear optics, and ω_p is called the pump frequency. We then first consider the case when ω_p is twice the mode eigenfrequency corresponding to degenerate parametric amplification [102]. The single-mode Hamiltonian (18) can be simplified using coefficient $\Lambda = \tau_0 T_{nn}/ml\omega_0^2$ as

$$H = \frac{p^2}{2m} + \frac{m\omega_0^2}{2} [1 + \Lambda \sin(2\omega_0 t)] q^2, \quad (21)$$

where ω_0 is the eigenfrequency and the mode suffix was omitted for simplicity. From this Hamiltonian, by taking into account the finite damping force and applying an external driving force, $F(t) = m g_0 \cos(\omega_0 t + \delta)$, the equation of

(a) Degenerate parametric amplification



(b) Non-degenerate parametric amplification

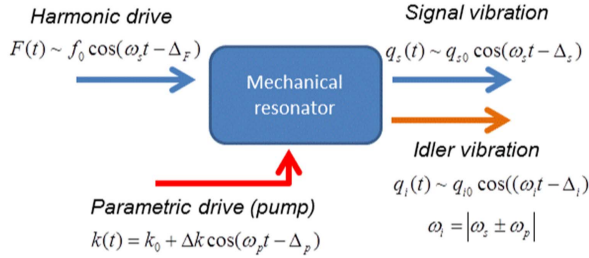


Figure 10. Schematic illustration of the two parametric amplification schemes. In both schemes, periodic force $F(t)$ (at ω_s) is applied externally to harmonically drive the resonator at around its resonance frequency to induce signal vibration. The vibration is then amplified/frequency-converted by parametric drive (pump), which is the sinusoidal modulation at ω_p of the force constant k from its average k_0 . (a) In degenerate parametric amplification, force constant k is modulated at twice the harmonic drive frequency $\omega_p = 2\omega_s$, leading to the amplification or damping of harmonically driven signal vibration $q_s(t)$ as described in 3.2. (b) In non-degenerate parametric amplification, the modulation can be made at an arbitrary frequency ω_p and the new frequency of vibration emerges at the sum or difference frequency $\omega_i = |\omega_s \pm \omega_p|$. To efficiently detect the ‘idler’ vibration $q_i(t)$, both the signal and idler should be within the bandwidth of some resonance modes.

motion is given by

$$\ddot{q} = -\frac{\omega_0}{Q}\dot{q} - \omega_0^2[1 + \Lambda \sin(2\omega_0 t)]q + g_0 \cos(\omega_0 t + \delta), \quad (22)$$

where Q is the quality factor. This equation is called the forced Mathieu equation. To find the time evolution of $q(t)$, we use a rotating frame approximation to introduce slowly varying amplitudes $c(t)$ and $s(t)$ as

$$q(t) = c(t) \cos(\omega_0 t) + s(t) \sin(\omega_0 t). \quad (23)$$

When $\Lambda < \gamma/\omega_0 = Q^{-1}$, equation of motion (22) can be then simplified as

$$\begin{aligned} \dot{c} &= -\frac{\gamma - \omega_0 \Lambda}{2}c + \frac{g_0}{2\omega_0} \sin \delta, \\ \dot{s} &= -\frac{\gamma + \omega_0 \Lambda}{2}s + \frac{g_0}{2\omega_0} \cos \delta. \end{aligned} \quad (24)$$

Therefore, the damping rate γ is effectively reduced by $\omega_0 \Lambda$ for the cosine quadrature, $c(t)$, whilst it is effectively increased by the same amount for the sine quadrature, $s(t)$. This is an important property of degenerated parametric

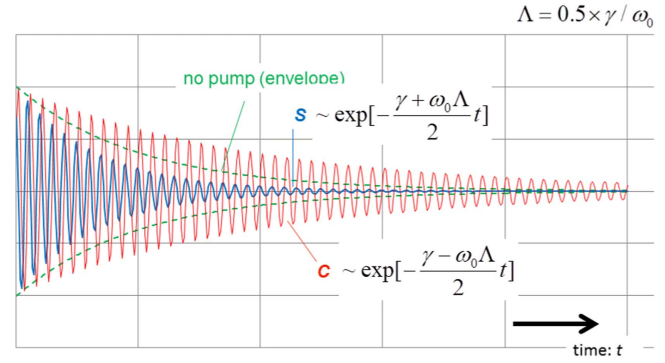


Figure 11. Calculated free decay curves (i.e. in the case $g_0 = 0$) of mechanical oscillation with parametric amplification. The sine component (blue line) decays more rapidly while the cosine component (red line) decays more slowly than in the case without the pump, whose amplitude envelope is shown by green dashed lines. When the parametric driving Λ becomes larger than the native damping rate γ/ω_0 , the cosine component develops to infinity, corresponding to the parametric oscillation.

amplification, where the cosine quadrature is amplified while the sine quadrature is damped (figure 11).

The steady state solution is easily calculated by assuming that c and s are time-independent. The vibration amplitude $\langle q^2(t) \rangle = \sqrt{c^2 + s^2}/2$ normalized by that with no pump, $\Lambda = 0$, gives the amplification gain expressed as

$$G = \frac{\langle q^2(t) \rangle}{\langle q^2(t) \rangle_{\Lambda=0}} = \sqrt{\frac{\sin^2 \delta}{(1 - \omega_0 \Lambda / \gamma)^2} + \frac{\cos^2 \delta}{(1 + \omega_0 \Lambda / \gamma)^2}}. \quad (25)$$

It has strong driving-phase (δ) dependence: the maximum gain is obtained at $\delta = \pi/2$ whilst the minimum gain (i.e. maximum damping) is at $\delta = 0$. The experimental results using a GaAs-based piezoelectric resonator are shown in figure 12 with the theoretical gain curve [equation (25)] [114].

The amplification gain for non-zero phase difference $\delta \neq 0$ becomes infinite when the parametric excitation approaches the threshold, $\Lambda \rightarrow \Lambda_{th} \equiv \gamma/\omega_0$. If the excitation becomes stronger than the threshold, the self-sustained oscillation is induced even without any harmonic driving, (i.e. $g_0 = 0$) [3, 23, 27, 115]. This regime is called ‘parametric oscillation’ and is also shown in figure 12(c). The oscillation amplitude in this case is limited not by energy dissipation as in the case of harmonic driving because the effective energy dissipation becomes negative. Instead, the nonlinearity becomes important and damps the vibration amplitude [23, 115].

The degenerate parametric oscillation can be described using the concept of broken discrete time translational symmetry. When $g_0 = 0$, equation (22) has a discrete time translational symmetry with the period π/ω_0 . In comparison, the solution corresponding to the parametric oscillation has the frequency ω_0 , which has the doubled period $2\pi/\omega_0$, breaking the discrete symmetry. Due to the broken symmetry, two independent solutions with π phase difference emerge. This fact causes a bistability in the oscillation states, which is applicable for binary signal processing [27, 115, 116].

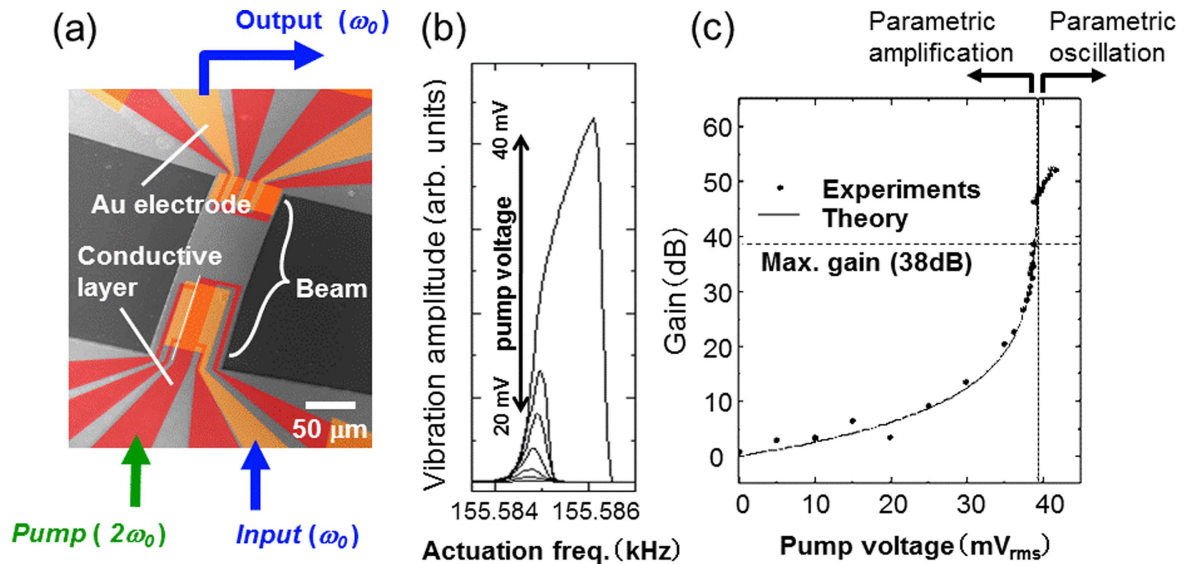


Figure 12. (a) Device structure and measurement setup used for the degenerate parametric amplification reported in [114]. Phase-locked pump and harmonic input voltages are applied on the conductive layer and one of the gate electrodes at $2\omega_0$ and ω_0 , respectively. The vibration amplitude at ω_0 is measured as the output voltage (signal) through another gate electrode using a lock-in amplifier. (b) The measured vibration amplitude when the pump and harmonic drive frequencies are swept around the resonance. The output voltage increases with increasing pump voltage. (c) The measured gain as a function of pump voltage. When pump excitation Λ approaches its threshold, $\Lambda_{th} \equiv \gamma/\omega_0$, the gain becomes large and unstable. The maximum gain of 38 dB was obtained just below the threshold of parametric oscillation.

3.3. Application of degenerate parametric amplification and oscillation.

One of the most impressive applications of parametric amplification is noise squeezing [102, 117, 118]. As seen in the previous subsection, two orthogonal vibration amplitudes, $c(t)$ and $s(t)$, have gain with opposite signs. When $c(t)$ is amplified (damped), $s(t)$ is damped (amplified). This is also the case for the amplification of quantum noise, i.e., the zero-point fluctuation. Using the parametric amplification, the quantum noise of one quadrature can be suppressed. Noise squeezing for mechanical resonators was first demonstrated for thermal noise by D Rugar [96]. Recently, quantum squeezing was demonstrated using microwave frequency radiation pressure [119, 120].

As a practical application of parametric amplification, atomic force microscopy with improved detection sensitivity was demonstrated [121]. Parametric amplification can improve the resonance linewidth of a mechanical cantilever, and the force sensitivity can be improved when the noise is dominated by that in external electronics. In contrast, in the cases where thermal vibration noise limits the sensitivity, both the signal and noise are amplified and the force sensitivity shows no improvement by parametric amplification.

Using the degenerate parametric oscillation of on-chip GaAs-based mechanical resonators, a parametron logic circuit has been proposed and memory operation [27] as well as a shift resistor [116] have been demonstrated. There are two oscillation phases allowed in parametric resonance at around the mechanical eigenfrequency. ‘Parametron’ computation uses the two oscillation phase states assigned to binary information ‘0’ and ‘1’. In the 1950’s, computation systems with several thousand electrical LC resonators were

constructed and used for practical calculations [115]. The same concept of binary logic operation was demonstrated using mechanical parametric resonators [27, 116]. The use of coupled GaAs cantilevers for mechanical logic elements was also proposed [57].

3.4. Quantum mechanical description of intermodal parametric coupling

Next, we consider the non-degenerate parametric resonator, which is realized by intermodal parametric coupling between two different vibration modes. The non-degenerate resonator can generate a different frequency of oscillation so that it can be applied to frequency conversion in practical applications. Furthermore, the resonator is significantly important in the application to quantum physics. As shown later, the pump excitation at the sum of two eigenmode frequencies can generate an entangled boson pair in the quantum regime. The scheme can therefore be one of the most promising techniques to prepare non-classical state of macroscopic objects.

The interaction can be derived from Hamiltonians (20) for a single beam ($H_{int} = \frac{\tau_{ext}}{2l} T_{nm} q_n q_m$), and also for coupled beams ($H_{int} = \tau_{ext} \lambda_c q_L q_H$ as described in appendix B). To describe the parametric intermodal coupling, it is instructive to describe the systems using a quantum mechanical phonon picture in analogy to quantum optics [122].

In quantum mechanics, q and p can be expressed by the creation and annihilation operators of a single phonon, a^\dagger and

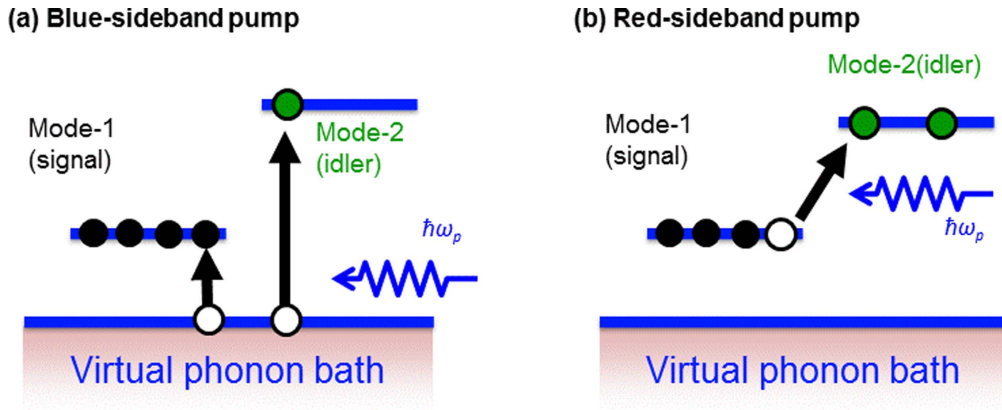


Figure 13. Schematic drawings of intermodal parametric pump processes using quantum mechanical phonon pictures. (a) The blue-sideband pump ($\omega_p = \omega_1 + \omega_2$) excites two phonons simultaneously in the two modes and induces non-degenerate parametric amplification. (b) The red-sideband pump ($\omega_p = \omega_2 - \omega_1$) transfers phonons from one mode to the other and causes the beam splitter interaction.

a, as

$$p_i = i\sqrt{\frac{m\omega_i\hbar}{2}}(a_i^\dagger - a_i), \quad q_i = \sqrt{\frac{\hbar}{2m\omega_i}}(a_i^\dagger + a_i) \quad (i = 1, 2), \quad (26)$$

where i is the mode index. Hamiltonian (20) becomes

$$H = \sum_{i=1,2} H_i + H_{\text{int}} \equiv H_0 + H_{\text{int}}$$

$$H_i = \hbar\omega_i \left(a_i^\dagger a_i + \frac{1}{2} \right), \quad H_{\text{int}} = 2\tau_{\text{ext}} A (a_1^\dagger + a_1) \times (a_2^\dagger + a_2). \quad (27)$$

Here, $A = \hbar T_{mn} / 8lm\sqrt{\omega_m\omega_n}$ for a single beam and $A = \hbar\lambda_c / 4m\sqrt{\omega_L\omega_H}$ for coupled beams as shown in appendix B, and mode suffixes 1 and 2 are used in both cases. We again consider the case where the tension is periodically modulated with t , i.e., $\tau_{\text{ext}}(t) = \tau_0 \cos \omega_p t$. By introducing the interaction representation, H_{int} becomes

$$\begin{aligned} H_{\text{int}} - \hat{H}_{\text{int}} &\equiv \exp[iH_0 t / \hbar] H_{\text{int}} \exp[-iH_0 t / \hbar] \\ &= 2\tau_0 A (a_1^\dagger e^{i\omega_1 t} + a_1 e^{-i\omega_1 t}) (a_2^\dagger e^{i\omega_2 t} + a_2 e^{i\omega_2 t}) \\ &\quad \times \cos(\omega_p t). \end{aligned} \quad (28)$$

We consider the two most important cases: $\omega_p = \omega_1 + \omega_2$ and $\omega_p = |\omega_2 - \omega_1|$, which are referred to as blue- and red-sideband pumps, respectively. By neglecting rapidly oscillating terms using rotating frame approximation, the interaction becomes

$$\begin{aligned} \hat{H}_{\text{int}} &\sim \tau_0 A (a_1^\dagger a_2^\dagger + a_1 a_2) \quad (\text{for } \omega_p = \omega_1 + \omega_2) \\ &\sim \tau_0 A (a_1^\dagger a_2 + a_1 a_1^\dagger) \quad (\text{for } \omega_p = |\omega_2 - \omega_1|) \end{aligned} \quad (29)$$

With the blue-sideband parametric pump, phonons are simultaneously generated (or annihilated) in both modes, which corresponds to non-degenerate parametric amplification (figure 13(a)). With the red-sideband parametric pump, one phonon is annihilated in one mode but one phonon is created in the other mode, which corresponds to the beam splitter interaction in quantum optics (figure 13(b)). Because the two modes have different frequencies, the beam splitter interaction converts the phonon frequency. Therefore, the

intermodal parametric coupling has two functions. One is parametric amplification and the other is frequency conversion, depending on which sideband frequency the pump excites.

3.5. Non-degenerate parametric amplification

The demonstration of the blue-sideband pump with a GaAs/AlGaAs single beam was first reported using detuned frequencies in a single mode [123] and later using two independent modes [42]. The experiments were performed by applying strain modulation at the sum of the pump frequencies ($\omega_p = \omega_1 + \omega_2$) as well as a harmonic drive (signal) at ω_1 . An idler signal at ω_2 generated by the blue-sideband pump was detected to confirm non-degenerate parametric amplification. Furthermore, a frequency multiplexing phonon computation scheme using higher-order idler generation was proposed [123]. Generating a new frequency from two corresponds to AND logic. By adequately choosing the signal and pump frequency and using destructive interference, the whole fundamental logic operation was demonstrated using a single-beam structure (figure 14).

The work was extended to perform experiments on two-mode thermal phonon squeezing. As described in 3.3, noise squeezing is based on the concept that the quadrature component of vibration noise is damped while the orthogonal one is amplified. The concept can be extended to the coupling of two oscillation modes using non-degenerate parametric amplification [122, 124]. Instead of the cross correlation between two orthogonal quadratures of a single mode in the degenerate case, the quadrature component of one mode has a correlation with the perpendicular component of the other mode. For example, the sine (cosine) noise component of the first mode has a correlation with the cosine (sine) noise component of the second mode.

For two vibrational modes, with the periodic tension modulation $\tau_{\text{ext}}(t) \sim \cos \omega_p t$, Hamiltonian (20) leads to the

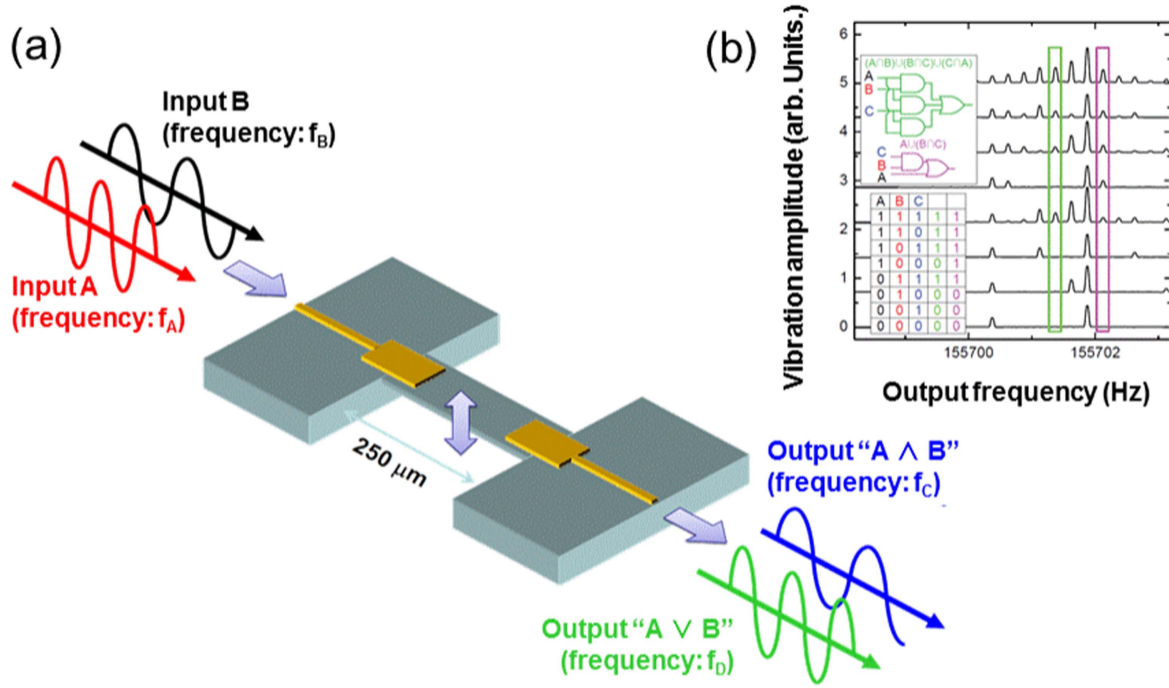


Figure 14. Schematic drawing of the concept of frequency-multiplexing phononic logic gates [123]. (a) Two-tone AC voltages applied to the resonator perform non-degenerate parametric amplification, generating different frequencies corresponding to the output of binary Boolean logic operation. (b) Examples of the output voltage spectra, demonstrating the three inputs majority (green) and (AND + OR) (purple) gates.

Langevin equations

$$\begin{aligned} \ddot{q}_1 + \gamma_1 \dot{q}_1 + \omega_1^2 q_1 + \Lambda \cos(\omega_p t) q_2 &= F_1^{th}(t) \\ \ddot{q}_2 + \gamma_2 \dot{q}_2 + \omega_2^2 q_2 + \Lambda \cos(\omega_p t) q_1 &= F_2^{th}(t), \end{aligned} \quad (30)$$

where $F_1^{th}(t)$ and $F_2^{th}(t)$ are thermal Langevin forces applied to the two modes. The pump frequency is given by $\omega_p = \omega_1 + \omega_2$, and Λ is the pump intensity, which is proportional to the strain modulation amplitude τ_0 . We can decompose the two mode variables into sine and cosine components as $q_i = c_i(t) \cos(\omega_i t) + s_i(t) \sin(\omega_i t)$, where c_i and s_i are slowly varying quadrature amplitudes of the i th mode and are measurable as the sine and cosine amplitude with a lock-in amplifier in experiments. The amplitude correlation in thermal noise becomes [43]

$$\langle s_i^2 \rangle = \langle c_i^2 \rangle = \frac{k_B T}{\omega_0^2 (1 - r^2)}. \quad (31)$$

$$\langle s_1 c_2 \rangle = \langle s_2 c_1 \rangle = -\frac{k_B T r}{\omega_0^2 (1 - r^2)}. \quad (32)$$

where $r = \Lambda / \omega_0 (\gamma_L + \gamma_H)$ is the normalized pump intensity and both ω_1 and ω_2 are replaced by ω_0 for simplicity by considering the case of $\omega_1 \approx \omega_2$. The equations show that the correlation increases with pump intensity and becomes unity when r approaches the threshold value, $r_{th} = 1$. Figure 15 shows the measured normalized cross-correlation $\langle s_1 c_2 \rangle / \sqrt{\langle s_1^2 \rangle \langle c_2^2 \rangle}$ for coupled GaAs/AlGaAs electromechanical resonators [43]. The dotted line shows the theoretical model calculation with the finite response time of the measurement system taken into account, showing good agreement with experiments.

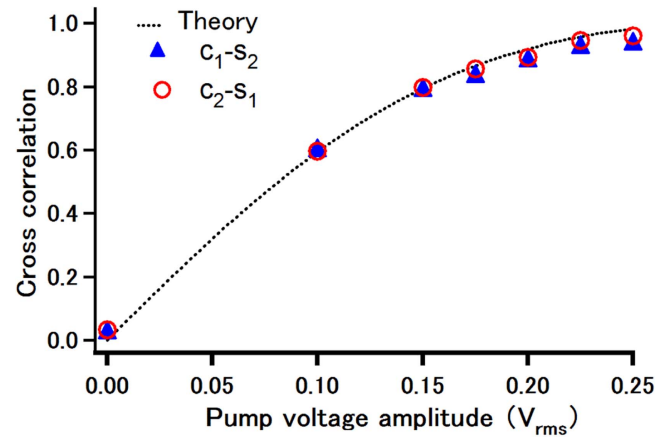


Figure 15. Cross correlation of the measured thermal noise component of two vibrational modes as a function of blue-sideband pump amplitude [43]. Red open circles and blue closed triangles show the experimental results, while the dotted line is the theoretical calculation. In the calculation, the threshold pump voltage of 0.29 V is assumed, which corresponds to the pump intensity: $r = 1$.

The concept of two-mode squeezing was initially introduced in quantum optics, where the quantum vacuum noise becomes correlated by the parametric pump [122, 124]. The pump translates the photon vacuum state into one consisting of a finite number of photons, and the quantum correlation over the two modes is generated. This correlated quantum state corresponds to the entangled photons and is important in the field of quantum information. The application of this scheme to parametric mechanical resonators in the quantum regime makes it possible to generate entangled phonon states in macroscopically distinguishable objects. Recently, the

generation of entangled states between phonons and microwave photons has been experimentally reported using the blue-sideband pump [119, 120].

When the pump amplitude becomes larger than the threshold, self-sustained oscillation is excited. Using a third resonance mode to effectively increase the pump amplitude in single beam geometry, all-mechanical phonon lasing operation was demonstrated [44]. This is another example of how the blue-sideband parametric pump can be used.

3.6. Beam-splitter interaction and frequency conversion

Now let us discuss the case of the red-sideband pump. As discussed in 3.4, the red-sideband pump generates the beam-splitter type interaction, which transfers a phonon in one mechanical mode to the other without changing the total phonon number. This operation can be expressed as $|n\rangle_1|m\rangle_2 \rightarrow |n \pm 1\rangle_1|m \mp 1\rangle_2$, where n and m is the initial phonon number in mode 1 and mode 2, respectively. These two modes have a different frequency, so that the interaction converts the phonon energy. In the case of classical oscillation, where the vibration is represented not by a phonon number state but by the superposition of different number states, i.e., a coherent state, the red-sideband pump can transfer the vibration energy from one mode to the other for frequency conversion in classical oscillation. Demonstrations of frequency conversion using micro/nanomechanical resonators are reported in [34, 36, 37].

When the frequency conversion rate becomes faster than the energy relaxation rate, phonons can stay in both modes, leading to their mixing. A red-sideband pump with enough intensity can strongly couple the two modes. This is technologically important in the sense that two modes with a different frequency can couple to each other and the coupling strength can be controlled by the intensity of the parametric pump.

We here theoretically describe the dynamics of two mechanical oscillation modes parametrically coupled to each other through the red-sideband pump. The equations of motion become

$$\begin{aligned} \ddot{q}_1 + \gamma_1 \dot{q}_1 + \omega_1^2 q_1 + \Gamma_1 \cos(\omega_p t) q_1 \\ + \Lambda \cos(\omega_p t) q_2 = F_0 \cos(\omega_s t - \delta) \\ \ddot{q}_2 + \gamma_2 \dot{q}_2 + \omega_2^2 q_2 + \Gamma_2 \cos(\omega_p t) q_2 \\ + \Lambda \cos(\omega_p t) q_1 = 0, \end{aligned} \quad (33)$$

where only mode 1 is harmonically driven by an external force [36]. The equation can be easily solved by applying rotating frame approximation when we assume that $\omega_p \sim \omega_2 - \omega_1$ and $\omega_s \sim \omega_1$. The resonance characteristics calculated using the parameters in [36] are shown in figure 16. As a function of pump and harmonic drive frequency, the vibration amplitude of the two modes shows the avoided crossing when the coupling rate becomes larger than the damping. The calculation shows excellent agreement with the experimental results.

The red-sideband pump has great importance in the field of optomechanics, where the coupling is made between

optical and mechanical modes. Compared to the number of thermally excited phonons, there are far fewer thermally excited photons because of the large energy quanta, so that their coupling can cool the mechanical mode by reducing the phonon number. The red-sideband-pump is induced by applying red-detuned laser light, and this laser cooling scheme is called sideband cooling. To achieve a phonon quantum ground state, a resolved-sideband condition is required [125], where the mechanical mode frequency is higher than the linewidth of the optical mode. Ground state cooling has been reported experimentally in both the microwave [126] and optical domains [127].

3.7. Application to electromechanically controlled phononic crystals

In condensed matters, the discrete electronic states localized at each atom position are laterally coupled to form energy bands where a crystal is constructed by an equally spaced array of atoms. The optical analog, i.e., photonic crystal, has recently been extensively studied by periodically modulating the reflective index in continuous media in artificial nanostructures. The passive and active control of photon propagation dynamics has been demonstrated by constructing photonic crystal waveguides. Similarly, the concept of the coupled mechanical resonator can be extended to form phononic crystals. The experimental study of phononic crystal was triggered in 1995 by experiments that confirmed the presence of band gaps in soundwave propagation through a 2D periodic arrangement of stainless steel cylinders [128]. By making periodically arranged holes in Si membranes, the formation of a band gap was also confirmed via surface acoustic wave (SAW) propagation in an on-chip device-based platform [129]. One of the most important motivations to use phononic crystals is the control of thermal transport [130]. Phononic crystals are also used to fabricate high frequency mechanical resonators [131] as well as the acoustic waveguides [132, 133].

The use of GaAs-based piezoelectric mechanical resonators as the building blocks of phononic crystals [134] allows the dynamic control of travelling acoustic waves [135, 136]. The locally generated strain induced by the mechanical vibration can modify the propagation dynamics.

Figure 17 shows a 1D phononic crystal waveguide fabricated using a GaAs/AlGaAs heterostructure. It consists of equally spaced membrane resonators. The acoustic wave is excited as the piezoelectrically induced mechanical vibration at one end, and the propagated acoustic vibration is detected at the other end of the waveguide both electrically and optically. The frequency response clearly shows the continuous propagation band as well as the band gap. By inserting a localized mechanical resonator at the middle of the waveguide, phononic wave propagation can be modulated. All-mechanical random access memory operation has also been demonstrated using a similar phononic waveguide structure [32]. Recently, GaAs-based phononic crystal for optomechanical applications has also been demonstrated [137].

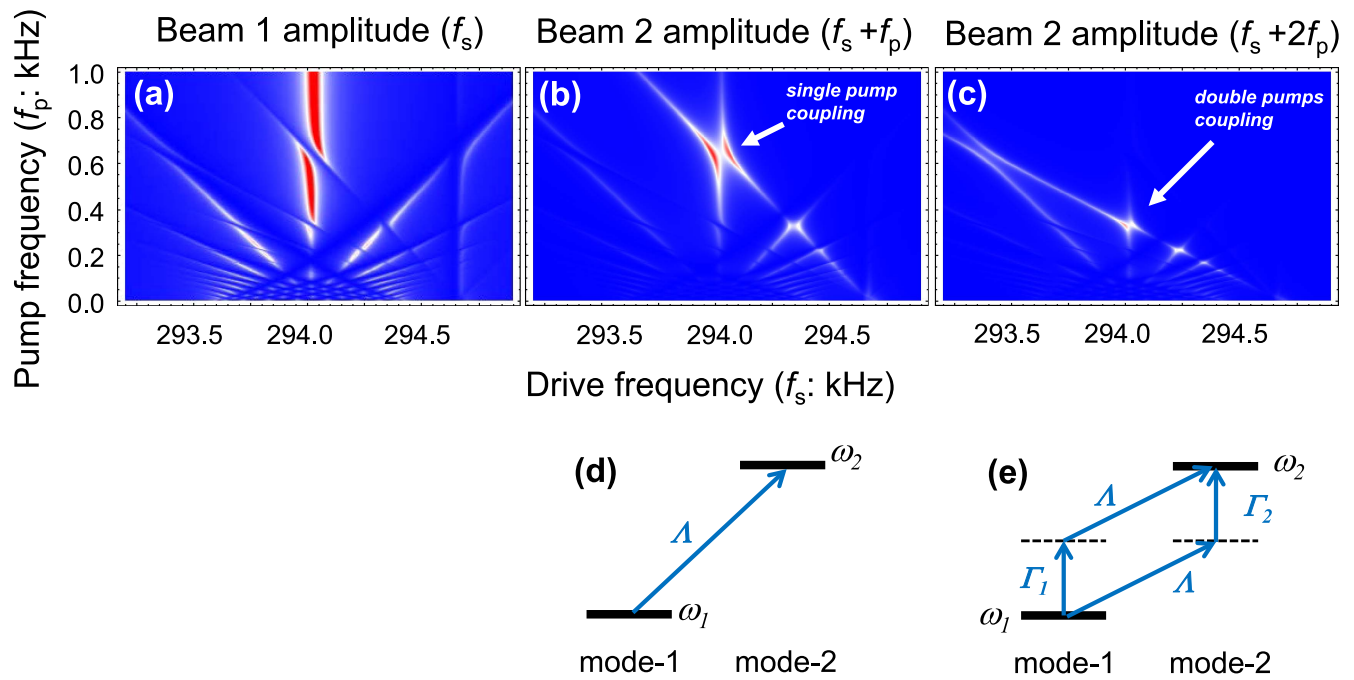


Figure 16. Numerical simulations of oscillation amplitudes of (a) beam 1 at drive frequency f_s , (b) beam 2 at first-order idler frequency $f_s + f_p$, and (c) beam 2 at second-order idler frequency $f_s + 2f_p$. The resonance frequencies of mode 1 and mode 2 are $f_1 = \omega_1/2\pi = 294.045$ kHz and $f_2 = \omega_2/2\pi = 294.645$ kHz, respectively. The avoided crossing is confirmed when pump frequency f_p becomes the red-sideband frequency $[f_2 - f_1]$ and its half frequency $[(f_2 - f_1)/2]$, corresponding to the diagrams shown in (d) and (e), respectively. [36].

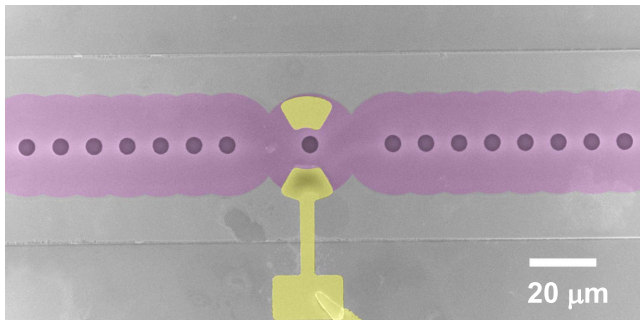


Figure 17. False-color SEM image of a phononic crystal embedding an electromechanical resonator [135]. The purple area is suspended and consists of an AlGaAs/n-GaAs heterostructure, where the acoustic vibration is propagating. The yellow areas are Shottky electrodes for the electromechanical control of the wave propagation. The waveguide is totally 1 mm long (not shown).

4. Carrier-mediated optomechanical systems

The integration of a mechanical resonator with optically active devices is also an advantage of III-V based electro-mechanical systems. GaAs/AlGaAs heterostructures are widely used for fabricating optoelectronic devices. One of the most pioneering works on III-V based optomechanical systems is the integration of a GaAs/AlGaAs laser with a micromechanical cantilever [54]. The mechanical modulation of laser emission was demonstrated using the cantilever as one mirror to form a laser cavity. The vibration modifies the cavity length, leading to the mechanical emission control. This experiment was the first demonstration of not only an

on-chip optomechanical device but also of state-of-the-art cavity optomechanics. As demonstrated by this example, the use of optomechanical devices allows the mechanical control of photonic devices. We here briefly show the results for carrier mediated optomechanics using GaAs/AlGaAs mechanical resonators [61–63], where similar optomechanical functions are incorporated without using an optical cavity.

The optical excitation of electron-hole pairs at the clamping point can create an electric field, leading to the formation of piezoelectric bending moment. Figure 18 shows the mechanical vibration characteristics measured through the optical drive and the dependence of vibration amplitude as a function of laser wavelength. When the excitation photon energy becomes larger than the band gap of GaAs, the vibration amplitude is drastically increased. A peak at the band edge (~ 850 nm) is visible, corresponding to the excitonic absorption. These results show that the photo-excited electron-hole pairs drive the mechanical vibration. The phase of the mechanical oscillation is reversed when an orthogonal cantilever is used, reflecting the fact that the piezoelectric force generated by the decomposed electron-hole pairs drives the mechanical motion.

The optopiezoelectric force on the mechanical mode allows the back-action effect in the mechanical resonant characteristics [61, 62]. The back-action effect on the harmonic oscillator is generally described by the following equations.

$$\ddot{q}(t) + \gamma\dot{q}(t) + \omega_0^2 q(t) = F_{ext}(t) + F_{BA}(t), \quad (34)$$

$$F_{BA}(t) = g \int_{-\infty}^t h(t-t')q(t')dt'. \quad (35)$$

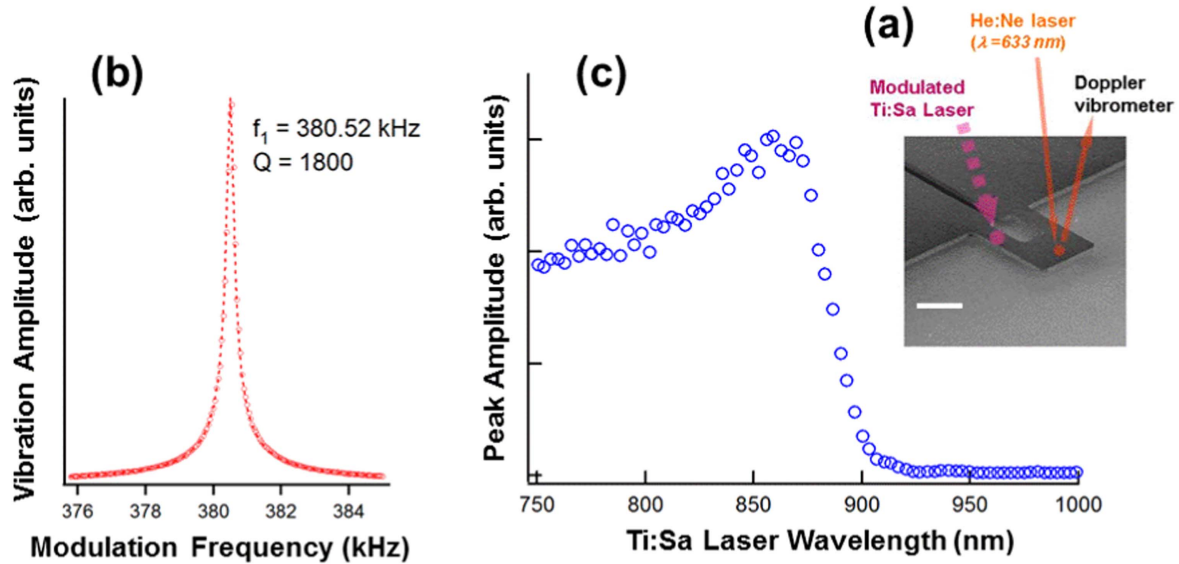


Figure 18. (a) The experimental setup for optopiezoelectric actuation. The intensity-modulated Ti:Sa laser is applied to the resonator to induce a periodic bending moment. The scale bar is $10 \mu\text{m}$. (b) The mechanical resonance characteristics measured at room temperature. (c) The vibration peak amplitude as a function of laser wavelength. The optical drive is effective when the photon energy is larger than the band gap of GaAs.

Here, $q(t)$ is the resonator displacement, $h(t)$ is the response function of the back action with the coupling constant g , where F_{ext} is the externally applied driving force, which is the thermal Langevin force when describing the Brownian motion of a mechanical resonator. We use the exponential response function $h(t) = \tau^{-1} \exp[-t/\tau]$, which is commonly used to describe the back action force with the response time constant τ . When the coupling constant g is much smaller than ω_0^2 , the renormalization of the resonance frequency and damping is derived from equation (34) as

$$\begin{aligned}\omega_0^2 \rightarrow \omega_{\text{eff}}^2 &= \omega_0^2 - \frac{g}{\tau^2 \omega_0^2 + 1}, \\ \gamma \rightarrow \gamma_{\text{eff}} &= \gamma + \frac{g\tau}{\tau^2 \omega_0^2 + 1}.\end{aligned}\quad (36)$$

Therefore, the damping can be both increased and decreased depending on the sign of the back action. For thermally driven resonators in particular, the increase of damping leads to the lowering of the effective mode temperature. The effective temperature, which can be measured as the area of the thermal noise power spectrum, is then given by $T_{\text{eff}} = \gamma T / \gamma_{\text{eff}}$, which can be increased/decreased by a negative/positive g value. Depending on the wavelength detuning from the exciton absorption peak, both cooling and heating were demonstrated using a GaAs/AlGaAs modulation-doped heterostructure [63]. The cantilever motion modifies the exciton absorption peak energy, modulating the absorption coefficient. The generated number of electron-hole pairs is then modulated by the cantilever motion, leading to the back-action effects. The present cooling efficiency of 50% [63] is expected to be improved by using the sharper absorption peak observed in quantum wells and quantum dots.

5. Hybridization with quantum low-dimensional electron systems

III-V compound semiconductor heterostructures are widely used to fabricate quantum low-dimensional (LD) structures. Their hybridization with mechanical resonators provides novel functionality both in mechanical and electronic devices. The extremely high force sensitivity of the mechanical resonator can be utilized for investigating the electron behavior in LD structures; on the other hand, the resonator motion can also modify the electronic state, leading to the mutual back-action force. In this section, the reported results that describe the coupling between mechanical modes and electronic states are briefly introduced.

5.1. Coupling with high-mobility 2D electron systems

One of the most important quantum LD systems in the study of electron transport is the high-mobility 2D electron systems (2DES). A variety of rich physics, such as quantum Hall effects and spin-related transport, have been studied using such systems. One of the pioneering works demonstrating the coupling of mechanical degrees of freedom with electron behavior was performed by Eisenstein *et al* [138, 139]. They studied the magnetization of a 2DES using a suspended piece of a 2DES sample. In mechanical systems, the magnetization of a 2DES, i.e., de Haas van Alphen effects, can be studied because the interaction between the magnetic moment of a 2DES and applied magnetic field generate torque. Related studies were later done by using similarly suspended structures [140–142] and more recently by using micromechanical resonators [143–145].

A 2DES was also used for detecting the mechanical motion. Integrating a 2DES FET as a strain sensor in a micromechanical resonator (for example figure 6(b)) allows

the sensitive detection of mechanical motion. As already cited, Beck *et al* developed a piezoresistive cantilever and proposed its use as a low-temperature AFM cantilever [89, 90]. The localized and delocalized electronic state transition in a 2DES was used as a sensitive strain sensor, and a very high strain gauge factor of 26 000 was reported [67]. This value is more than two orders of magnitude larger than that of a Si piezoresistive cantilever. The strain induced by the mechanical beam motion causes the modulation of electronic states, leading to the order-disorder transition in the 2DES, and the conductance is highly sensitive to the motion-induced transition.

The motion-induced order-disorder transition causes electron transport along the strain gradient within the sample. This electron transport generates a magneto-piezo voltage, which is highly sensitive to the filling factor. At very low temperature, the intrinsic Q of the cantilever becomes about 10^6 , where the dominant source of energy dissipation is ohmic loss caused by the electron transport. The increase in Q at the edges of the quantum Hall plateau, where localized electronic states suppress the ohmic loss, shows the back-action of the 2DES onto the mechanical motion [67, 68]. Similar phenomena were also observed in the propagation characteristics of surface acoustic waves [146]. Hybrid structures integrating a 2DES in a micromechanical resonator are also studied in [147] and [148]. Structures integrating superconductor-semiconductor weak link junctions for motion detection are studied in [149–151].

5.2. Coupling with 0D quantum structures

The coupling of mechanical degrees of freedom with artificially localized electrons has also been studied not only with semiconductor-based single-electron transistors (SETs) and quantum QPCs [69, 70, 92–94] but also with hybrid structures with normal metal [93] and superconductor [152, 153] SETs, for which highly sensitive motion detection was reported. The 0D systems with a small number of electrons, i.e., QDs, have also been studied, mainly using semiconductor-based structures [70]. An example of the device structures is shown in figure 6(c). The use of 0D transport, i.e., the quantized conductance through a QPC, for strain sensing and, recently, motion detection using photoluminescence in QD structures were reported. These works are based on the strain-mediated coupling between electronic states and mechanical motion.

As in the 2DES, electron-induced back-action has also been confirmed in a hybrid device comprising a top-down semiconductor QD and mechanical resonator. An increase in energy dissipation as well as the amplification of mechanical motion was observed. The bias current flowing through the QD amplifies the mechanical vibration, which might be applicable to current-injected phonon lasers in the future [154, 155].

Experiments using bottom-up self-organized quantum dots [80, 82] as well as theoretical works describing the hybrid devices have also been reported [156–159]. One of the main targets is the realization of a Jaynes–Cummings model. Phonon-based cavity-QED experiments can be performed

using a QD and mechanical resonator as a quantum two-level system and harmonic oscillator, respectively.

6. Conclusions

The high crystalline quality and piezoelectric properties of epitaxially grown GaAs enables the fabrication of high-performance mechanical resonators for various applications. In particular, the parametric resonators can be used for signal processing, from frequency converters and high-accuracy timing devices to electromechanical logic.

By integrating the high functionalities of GaAs/AlGaAs optoelectronic micro and nanostructures into mechanical resonators, new device concepts have been introduced. The high crystalline quality of single-crystal heterostructures allows highly reliable and stable opto- and electromechanical operation. Although the material system of only GaAs/AlGaAs is discussed in this article, other compound semiconductor materials are also promising for the opto- and electromechanical applications. For instance, highly piezoelectric nitride semiconductors have recently been studied for high-frequency mechanical resonator applications as well as InP-based structures allowing telecom band optomechanical operation.

Finally, the integration with quantum low-dimensional systems is discussed. The hybrid structures provide new techniques to artificially manipulate quantum electronic states as well as to achieve their mutual coupling. Reversely, the quantum structures modify the mechanical resonance characteristics through back-action.

The studies shown here are basically ‘proof of concept’ experiments and further improvements are required to apply the concepts to real applications. For example, the QD-mechanical resonator hybrid device has very high position sensitivity only at cryogenic temperatures. To make it working as a practical device, a high performance room temperature SET/QD is required. Such a device has been demonstrated so far only using Si-based transistors [160], so that the heterogeneous integration of III-V and Si-based devices might play an important role.

One important key improvement is to increase the resonance frequency into the GHz region. Practical device applications such like nonlinear signal processing and highly stable timing devices require the operation at the frequency region. The resonance frequency can be increased by reducing the structure size as described in section 2.1 but the confinement of mechanical vibration becomes insufficient due to the reduced acoustic mismatch between the flexural beam motion and the surface acoustic wave. Different designs of mechanical resonators, such as bulk acoustic resonators [86, 87] and phononic crystal wave guide resonators [137] are promising to overcome the difficulties. In addition, the quality factor lowered by the insufficient acoustic mismatch can be improved by using strained layer heterostructures. The use of compound semiconductors is advantageous for strain engineering as already described [52, 53, 77].

Also in the application of quantum hybrid devices to quantum information technology, the electronic and mechanical systems have different energy scales at present but increasing the resonance frequency into the GHz region put single phonons and electrons into superposed and/or entangled states. There are several activities in this direction, opening up a new research field of electron-phonon hybrid quantum systems.

Acknowledgments

I thank our collaborators, Daiki Hatanaka, Imran Mahboob, Ryuichi Ohta, Hajime Okamoto, Yuma Okazaki, Koji Onomitsu, and Takayuki Watanabe, for their help and support as well as for making their data available to me. This work was partly supported by MEXT KAKENHI (Grant No. JP15H05869 and JP15K21727).

Appendix A

To describe the parametric resonators, we start from the expression of the Euler–Bernoulli equation using Hamiltonian formalism:

$$H_0[\Pi, z] = \int_0^l \left[\frac{\Pi^2}{2\rho A} + \frac{EI_y}{2} \left(\frac{\partial^2 z}{\partial x^2} \right)^2 \right] dx.$$

Here, $\Pi(x, t) = \rho A \delta \dot{z}(x, t)$ is the momentum density, $A = dw$ is the area of the beam cross section, and $I_y = d^3w/12$ is the moment of inertia. The first term in the square brackets gives the kinetic energy and the second one gives the potential energy induced by the elastic deformation of the beam. Equation (1) as well as the definition of $\Pi(x, t)$ can be derived from the canonical equations of motion $\dot{z}(x) = \delta H_0 / \delta \Pi(x)$ and $\dot{\Pi}(x) = -\delta H_0 / \delta z(x)$ by assuming the appropriate boundary condition, for example, equations (4) or (5). The displacement and the momentum density, which also generally satisfy the same boundary condition, can be expanded by the mode function $u_m(x)$ as

$$z(x, t) = \sum_m q_m(t) u_m(x),$$

$$\Pi(x, t) = \quad \quad \quad l$$

Then, using the orthonormal condition [equation (10)], the Hamiltonian can be expressed by mode displacement $q_m(t)$ and momentum variables $p_m(t) = m\dot{q}_m$ as

$$H_0[p, q] = \sum_m \left(\frac{p_m^2}{2m} + \frac{m\omega_m^2 q_m^2}{2} \right).$$

The system can be regarded as an ensemble of independent harmonic oscillators.

Then, we take into account the effect of beam tension. Because the propagation velocity of longitudinal elastic waves (i.e., LA phonons) is much higher than the time scale of the mechanical oscillation, the tension can be assumed to be position-independent. The modified Hamiltonian is given

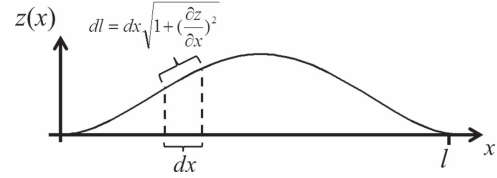


Figure 19. Schematic drawing showing the beam extension induced by its displacement.

by

$$H[\Pi, z] = \int_0^l \left[\frac{\Pi^2}{2\rho A} + \frac{EI_y}{2} \left(\frac{\partial^2 z}{\partial x^2} \right)^2 \right] dx + \frac{\tau^2 l}{2EA}.$$

Here, tension τ is decomposed into two parts: an externally applied one and that induced by beam vibration (figure 19), i.e.,

$$\tau(t) = \tau_{ext}(t) + \frac{EA}{l} \left[\int_0^l \sqrt{1 + \left(\frac{\partial z}{\partial x} \right)^2} dx - l \right]$$

First, let us consider the case when no external tension is applied. The Hamiltonian becomes

$$H[\Pi, z] = \int_0^l \left[\frac{\Pi^2}{2\rho A} + \frac{EI_y}{2} \left(\frac{\partial^2 z}{\partial x^2} \right)^2 \right] dx + \frac{EA}{8l} \left[\int_0^l \left(\frac{\partial z}{\partial x} \right)^2 dx \right]^2$$

up to the fourth order in z , where the z -independent term is neglected because it does not affect the beam dynamics. By expanding $z(x, t)$ using the normal mode wave functions $u_m(x)$, we finally obtain the important expression

$$H[\Pi, z] = H_0[p, q] + \frac{EA}{8l^3} \left(\sum_{m,n} T_{mn} q_m(t) q_n(t) \right)^2,$$

$$T_{mn} = l \int_0^l u'_m(x) u'_n(x) dx.$$

T_{mn} is a dimensionless matrix given by

$$T_{mn} = \begin{pmatrix} 12.30 & 0 & 9.73 & 0 & \\ 0 & 46.05 & 0 & 17.13 & \dots \\ 9.73 & 0 & 98.90 & 0 & \\ 0 & 17.13 & 0 & 171.59 & \\ & & & \vdots & \ddots \end{pmatrix}$$

for doubly clamped beam resonators. The tension generated by the beam oscillation gives fourth-order nonlinearity. If only the n th mode has finite vibration amplitude, the Hamiltonian corresponds to the well-known nonlinear Duffing oscillator [1, 3, 23, 110]:

$$H_n = \frac{p_n^2}{2m} + \frac{m\omega_n^2 q_n^2}{2} + \frac{EAT_{nn} q_n^4}{8l^3}.$$

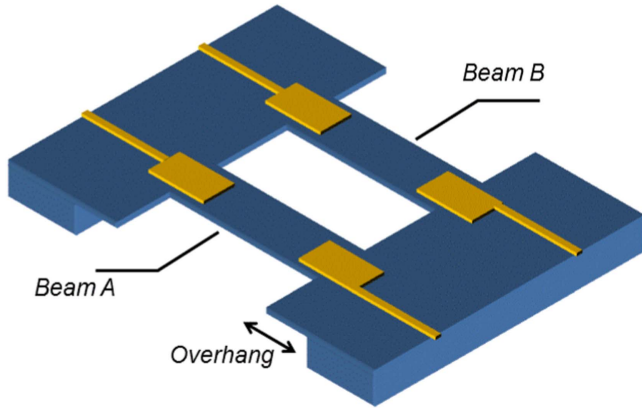


Figure 20. Schematic drawing showing a paired-beam resonator. The yellow part shows the Schottky electrodes to drive and detect the mechanical motion as well as the resonance frequency modulation, while the embedded conductive layer is grounded (not shown for simplicity). The two beams, A and B, are structurally coupled through the overhang [36].

Next, let us consider the case when tension τ_{ext} is externally applied. The lowest order contribution is given by

$$H[\Pi, z] = H_0[p, q] + \frac{\tau_{ext}}{2l} \sum_{m,n} T_{mn} q_m(t) q_n(t).$$

When only the n th mode is taken into account, the Hamiltonian (18) is obtained:

$$H_n = \frac{p_n^2}{2m} + \frac{(m\omega_n^2 + \tau_{ext}T_{nn}/l)q_n^2}{2}.$$

Appendix B

Tension-induced mode coupling can also be derived for paired-beam resonators [36]. Figure 20 shows an example of coupled structures with electrodes to drive and detect the mechanical motion. Two parametric resonators are structurally coupled through an overhang, which is formed by sacrificial etching.

The Hamiltonian of the two coupled beams, A and B, is given by

$$H = \frac{p_A^2}{2m} + \frac{(m\omega_A^2 + \tau_{ext}T_{AA}/l)q_A^2}{2} + \frac{p_B^2}{2m} + \frac{m\omega_B^2 q_B^2}{2} + \frac{cm}{2}(q_A - q_B)^2$$

The last term gives the structural coupling between the two beams induced by the overhang, and the external tension modulation is assumed to be applied only to beam A as an electric voltage, corresponding to the term $\tau_{ext}T_{AA}/l$. Because of the structural coupling, each normal mode receives finite contributions from both beams even when they have a different eigenfrequency (i.e., $\omega_A \neq \omega_B$).

The variables in this equation can be transformed into normal mode ones by using the following orthonormal

transformation:

$$\begin{pmatrix} x_L \\ x_H \end{pmatrix} = U \begin{pmatrix} x_A \\ x_B \end{pmatrix}, \quad \begin{pmatrix} p_L \\ p_H \end{pmatrix} = U \begin{pmatrix} p_A \\ p_B \end{pmatrix},$$

$$U = \frac{1}{\sqrt{2h}} \begin{pmatrix} \sqrt{h+d} & \sqrt{h-d} \\ \sqrt{h-d} & -\sqrt{h+d} \end{pmatrix}, \quad d = \frac{\omega_B^2 - \omega_A^2}{2},$$

$$h = \sqrt{c^2 + d^2},$$

$$\omega_L^2 = \omega_A^2 + c + d - h, \quad \omega_H^2 = \omega_A^2 + c + d + h.$$

This leads to the new Hamiltonian with normal mode variables:

$$H = \frac{p_L^2}{2m} + \frac{m\omega_L^2 q_L^2}{2} + \frac{p_H^2}{2m} + \frac{m\omega_H^2 q_H^2}{2} + \tau_{ext} \left(\frac{\lambda_L}{2} q_L^2 + \frac{\lambda_H}{2} q_H^2 + \lambda_c q_L q_H \right),$$

where the coefficients λ_L , λ_H , and λ_c are given by

$$\lambda_L = U_{11}^2 T_{AA}/l, \quad \lambda_H = U_{21}^2 T_{AA}/l,$$

$$\lambda_c = U_{11} U_{21} T_{AA}/l.$$

where L and H are indices specifying low- and high-frequency diagonalized modes, respectively. Although the initial form has only the parametric modulation of beam A's force constant, the transformed Hamiltonian includes the parametric modulation of both normal modes, as well as the intermodal coupling. This Hamiltonian is the combined form of (18) and (20), and it shows that both intramodal (i.e., the degenerate parametric) and intermodal (non-degenerate parametric) coupling can be induced by the strain, with the coefficients λ_L/λ_H and λ_c , respectively. The strain applied to beam A modifies the two lowest normal modes, leading to the frequency modulation in both modes as well as their intermixing. Nonlinear dynamics in coupled resonators have also been studied in other systems [161–163].

References

- [1] Cleland A N 2003 *Foundations of Nanomechanics* (Berlin Heidelberg: Springer)
- [2] Ekinci K L and Roukes M L 2005 Nanoelectromechanical systems *Rev. Sci. Instr.* **76** 061101
- [3] Younis M I 2011 *MEMS Linear and Nonlinear Statics and Dynamics* (New York: Springer)
- [4] Schmid S, Villanueva L G and Roukes M L 2016 *Fundamentals of Nanomechanical Resonators* (Switzerland: Springer)
- [5] Wiesendanger R 1994 *Scanning Probe Microscopy and Spectroscopy* (Cambridge: Cambridge University Press)
- [6] Nguyen C 2007 MEMS technology for timing and frequency control *IEEE Trans. Ultrason. Ferroelect. Freq. Contr.* **54** 251–70
- [7] Huang X M H, Zorman C A, Mehregany M and Roukes M L 2003 Nanodevice motion at microwave frequencies *Nature* **421** 496
- [8] Chaste J, Eichler A, Moser J, Ceballos G, Rurali R and Bachtold A 2012 A nanomechanical mass sensor with yoctogram resolution *Nat. Nanotechnol.* **7** 300–3
- [9] Gaidarzhy A, Imboden M, Mohanty P, Rankin J and Sheldon B W 2007 High quality factor gigahertz frequencies

- in nanomechanical diamond resonators *Appl. Phys. Lett.* **91** 203503
- [10] Tomes M and Carmon T 2009 Photonic micro-electromechanical systems vibrating at X-band (11 GHz) rates *Phys. Rev. Lett.* **102** 113601
- [11] Rinaldi M, Zuniga C, Zuo C and Piazza G 2010 Super-high-frequency two-port AlN contour-mode resonators for RF applications *IEEE Trans. Ultrason. Ferroelect. Freq. Contr.* **57** 38–45
- [12] Ding L, Baker C, Senellart P, Lemaitre A, Ducci S, Leo G and Favero I 2010 High frequency GaAs nano-optomechanical disk resonator *Phys. Rev. Lett.* **105** 263903
- [13] Ding L, Baker C, Senellart P, Lemaitre A, Ducci S, Leo G and Favero I 2011 Wavelength-sized GaAs optomechanical resonators with gigahertz frequency *Appl. Phys. Lett.* **98** 113108
- [14] Tao Y, Boss J M, Moores B A and Degen C L 2014 Single-crystal diamond nanomechanical resonators with quality factors exceeding one million *Nat. Commun.* **5** 3638
- [15] Moser J, Eichler A, Guttlinger J, Dykman M I and Bachtold A 2014 Nanotube mechanical resonators with quality factors of up to 5 million *Nat. Nanotechnol.* **9** 1007
- [16] Kermany A R, Brawley G, Mishra N, Sheridan E, Bowen W P and Iacopi F 2014 Microresonators with Q-factors over a million from highly stressed epitaxial silicon carbide on silicon *Appl. Phys. Lett.* **104** 081901
- [17] Verbridge S S, Craighead H G and Parpia J M 2008 A megahertz nanomechanical resonator with room temperature quality factor over a million *Appl. Phys. Lett.* **92** 013112
- [18] Roukes M L 2000 Nanoelectromechanical systems *Technical Digest of the 2000 Solid-State Sensor and Actuator Workshop* pp 1–10
- [19] Poot M and van der Zant H S J 2012 Mechanical systems in the quantum regime *Phys. Rep.* **511** 273
- [20] Chan J, Alegre T P M, Safavi-Naeini A H, Hill J T, Krause A, Groblacher S, Aspelmeyer M and Painter O 2011 Laser cooling of a nanomechanical oscillator into its quantum ground state *Nature* **478** 7367
- [21] O'Connell A D *et al* 2010 Quantum ground state and single-phonon control of a mechanical resonator *Nature* **464** 7289
- [22] Teufel J D, Donner T, Li D L, Harlow J W, Allman M S, Cicak K, Sirois A J, Whittaker J D, Lehnert K W and Simmonds R W 2011 Sideband cooling of micromechanical motion to the quantum ground state *Nature* **475** 7356
- [23] Lifshitz R and Cross M C 2008 Nonlinear dynamics of nanomechanical and micromechanical resonators *Review of Nonlinear Dynamics and Complexity* (Weinheim: Wiley-VCH)
- [24] Dykman M (ed) 2012 *Fluctuating Nonlinear Oscillators* (Oxford: Oxford Univ. Press)
- [25] Badzey R L, Zolfagharkhani G, Gaidarzhy A and Mohanty P 2004 A controllable nanomechanical memory element *Appl. Phys. Lett.* **85** 3587–9
- [26] Badzey R L and Mohanty P 2005 Coherent signal amplification in bistable nanomechanical oscillators by stochastic resonance *Nature* **437** 995–8
- [27] Mahboob I and Yamaguchi H 2008 Bit storage and bit flip operations in an electromechanical oscillator *Nature Nanotechnol.* **6** 726–32
- [28] Guerra D N, Bulsara A R, Ditto W L, Sinha S, Murali K and Mohanty P 2010 A noise-assisted reprogrammable nanomechanical logic gate *Nano Lett.* **10** 1168–71
- [29] Venstra W J, Westra H J R and van der Zant H S J 2010 Mechanical stiffening, bistability, and bit operations in a microcantilever *Appl. Phys. Lett.* **97** 193107
- [30] Noh H, Shim S B, Jung M, Khim Z G and Kim J 2010 A mechanical memory with a dc modulation of nonlinear resonance *Appl. Phys. Lett.* **97** 033116
- [31] Yao A and Hikiyara T 2014 Logic-memory device of a mechanical resonator *Appl. Phys. Lett.* **105** 123104
- [32] Hatanaka D, Mahboob I, Onomitsu K and Yamaguchi H 2014 Mechanical random access memory in a phonon circuit *Appl. Phys. Express* **7** 125201
- [33] Mahboob I, Froitier C and Yamaguchi H 2010 A symmetry-breaking electromechanical detector *Appl. Phys. Lett.* **96** 213103
- [34] Mahboob I, Nishiguchi K, Okamoto H and Yamaguchi H 2012 Phonon-cavity electromechanics *Nature Phys.* **8** 387
- [35] Yamaguchi H, Okamoto H and Mahboob I 2012 Coherent control of micro/nanomechanical oscillation using parametric mode mixing *Appl. Phys. Express* **5** 014001
- [36] Okamoto H, Gourgout A, Chang C-Y, Onomitsu K, Mahboob I, Chang E Y and Yamaguchi H 2013 Coherent phonon manipulation in coupled mechanical resonators *Nature Phys.* **9** 480
- [37] Faust T, Rieger J, Seitner M J, Kotthaus J P and Weig E M 2013 Coherent control of a classical nanomechanical two-level system *Nature Phys.* **9** 485
- [38] Liu C H, Kim I S and Lauthon L J 2015 Optical control of mechanical mode-coupling within a MoS₂ resonator in the strong-coupling regime *Nano Lett.* **15** 6727–31
- [39] Mathew J P, Patel R N, Borah A, Vijay R and Deshmukh M M 2016 Dynamical strong coupling and parametric amplification of mechanical modes of graphene drums *Nature Nanotech.* **11** 747
- [40] Okamoto H, Schilling R, Schutz H, Sudhir V, Wilson D J, Yamaguchi H and Kippenberg T J 2016 A strongly coupled Λ -type micromechanical system *Appl. Phys. Lett.* **108** 153105
- [41] Zhu D *et al* 2017 Coherent phonon Rabi oscillations with a high-frequency carbon nanotube phonon cavity *Nano Lett.* **17** 915–21
- [42] Mahboob I, Wilmart Q, Nishiguchi K, Fujiwara A and Yamaguchi H 2011 Wide-band idler generation in a GaAs electromechanical resonator *Phys. Rev. B* **84** 113411
- [43] Mahboob I, Okamoto H, Onomitsu K and Yamaguchi H 2014 Two-mode thermal-noise squeezing in an electromechanical resonator *Phys. Rev. Lett.* **113** 167203
- [44] Mahboob I, Nishiguchi K, Fujiwara A and Yamaguchi H 2013 Phonon lasing in an electromechanical resonator *Phys. Rev. Lett.* **110** 127202
- [45] Boisen A, Dohn S, Keller S S, Schmid S and Tenje M 2011 Cantilever-like micromechanical sensors *Rep. Prog. Phys.* **74** 036101
- [46] Stowe T D, Yasumura K, Kenny T W, Botkin D, Wago K and Rugar D 1997 Attonewton force detection using ultrathin silicon cantilevers *Appl. Phys.* **71** 288–90
- [47] Fritz J, Baller M K, Lang H P, Rothuizen H, Vettiger P, Meyer E, Guntherodt H J, Gerber C and Gimzewski J K 2000 Translating biomolecular recognition into nanomechanics *Science* **288** 316–8
- [48] Rugar D, Budakian R, Mamin H J and Chui B W 2004 Single spin detection by magnetic resonance force microscopy *Nature* **430** 329–32
- [49] Prinz V Y, Seleznev V A, Gutakovskiy A K, Chekhovskiy A V, Preobrazhenskii V V, Putyato M A and Gavrilova T A 2000 Free-standing and overgrown InGaAs/GaAs nanotubes, nanohelices and their arrays *Physica E* **6** 828–31
- [50] Seleznev V A, Yamaguchi H, Hirayama Y and Prinz V Y 2003 Single-turn GaAs/InAs nanotubes fabricated using the supercritical CO₂ drying technique *Jpn. J. Appl. Phys.* **42** L791–4
- [51] Vaccaro P O, Kubota K, Fleischmann T, Saravanan S and Aida T 2003 Valley-fold and mountain-fold in the micro-origami technique *Microelectromechanics Journal* **34** 447–9

- [52] Yamaguchi H, Kato K, Nakai Y, Onomitsu K, Warisawa S and Ishihara S 2008 Improved resonance characteristics of GaAs beam resonators by epitaxially induced strain *Appl. Phys. Lett.* **92** 251913
- [53] Onomitsu K, Mitsuhashi M, Yamamoto H and Yamaguchi H 2013 Ultrahigh-Q micromechanical resonators by using epitaxially induced tensile strain in GaNAs *Appl. Phys. Express* **6** 111201
- [54] Ukita H, Uenishi Y and Tanaka H 1993 A Photo-microdynamical system with a mechanical resonator monolithically integrated with laser diodes on gallium arsenide *Science* **260** 786–9
- [55] Beck R G, Eriksson M A, Westervelt R M, Campman K L and Gossard A C 1996 Strain-sensing cryogenic field-effect transistor for integrated strain detection in GaAs/AlGaAs microelectromechanical systems *Appl. Phys. Lett.* **68** 3763–5
- [56] Beck R G, Eriksson M A, Topinka M A, Westervelt R M, Maranowski K D and Gossard A C 1998 GaAs/AlGaAs self-sensing cantilevers for low temperature scanning probe microscopy *Appl. Phys. Lett.* **73** 1149
- [57] Masmanidis S C, Karabalin R B, Vlaminck I D, Borghs G, Freeman M R and Roukes M L 2007 Multifunctional nanomechanical systems via tunably coupled piezoelectric actuation *Science* **317** 780–3 (2007)
- [58] Brueckner K, Niebelschuetz F, Tonisch K, Michael S, Dadgar A, Krost A, Cimalla V, Ambacher O, Stephan R and Hein M A 2008 Two-dimensional electron gas based actuation of piezoelectric AlGaIn/GaN microelectromechanical resonators *Appl. Phys. Lett.* **93** 173504
- [59] Faucher M *et al* 2009 Amplified piezoelectric transduction of nanoscale motion in gallium nitride electromechanical resonators *Appl. Phys. Lett.* **94** 233506
- [60] Karabalin R B, Matheny M H, Feng X L, Defay E, Le Rhun G, Marcoux C, Hentz S, Andreucci P and Roukes M L 2009 Piezoelectric nanoelectromechanical resonators based on aluminum nitride thin films *Appl. Phys. Lett.* **95** 103111
- [61] Okamoto H, Ito D, Onomitsu K, Sanada H, Gotoh H, Sogawa T and Yamaguchi H 2011 Vibration amplification, damping, and self-oscillations in micromechanical resonators induced by optomechanical coupling through carrier excitation *Phys. Rev. Lett.* **106** 036801
- [62] Okamoto H, Ito D, Watanabe T, Onomitsu K, Sanada H, Gotoh H, Sogawa T and Yamaguchi H 2011 Carrier-mediated optomechanical coupling in GaAs cantilevers *Phys. Rev. B* **84** 014305
- [63] Okamoto H, Watanabe T, Ohta R, Onomitsu K, Gotoh H, Sogawa T and Yamaguchi H 2015 Cavity-less on-chip optomechanics using excitonic transitions in semiconductor heterostructures *Nature Comm.* **6** 8478
- [64] Landau L D and Lifshitz E M 1986 *Theory of Elasticity* 3rd edn (Oxford: Butterworth-Heinemann)
- [66] Mahboob I, Okamoto H, Ueki M and Yamaguchi H 2006 Electron phase modulation in a suspended InAs/AlGaSb nanomechanical beam *Appl. Phys. Lett.* **89** 192106
- [67] Yamaguchi H, Okamoto H, Maruta Y, Ishihara S, Miyashita S and Hirayama Y 2007 Giant magneto-piezoresistance and internal friction in a two-dimensional electron system *Jpn. J. Appl. Phys.* **46** 658–60
- [68] Yamaguchi H, Okamoto H, Ishihara S and Hirayama Y 2012 Motion detection of a micromechanical cantilever through magneto-piezovoltage in two-dimensional electron systems *Appl. Phys. Lett.* **100** 012106
- [69] Okazaki Y, Mahboob I, Onomitsu K, Sasaki S and Yamaguchi H 2013 Quantum point contact displacement transducer for a mechanical resonator at sub-Kelvin temperatures *Appl. Phys. Lett.* **103** 192105
- [70] Okazaki Y, Mahboob I, Onomitsu K, Sasaki S and Yamaguchi H 2016 Gate-controlled electromechanical backaction induced by a quantum dot *Nature Commun.* **7** 11132
- [71] Faucher M, Cordier U, Werquin M, Buchaillet L, Gaquière C and Théron D 2012 Electromechanical transconductance properties of a GaN MEMS resonator with fully integrated HEMT transducers *IEEE J. Microelectromech. Syst.* **21** 370–8
- [72] Pruessner M W, King T T, Kelly D P, Grover R, Calhoun L C and Ghodssi R 2003 Mechanical property measurement of InP-based MEMS for optical communications *Sensors Actuators A* **105** 190–200
- [73] Pruessner M W, Siwak N, Amarnath K, Kanakaraju S, Chuang W-H and Ghodssi R 2006 End-coupled optical waveguide MEMS devices in the indium phosphide material system *J. Micromech. Microeng.* **16** 832–42
- [74] Yamaguchi H, Miyashita S and Hirayama Y 2003 Microelectromechanical displacement sensing using InAs/AlGaSb heterostructures *Appl. Phys. Lett.* **82** 394–6
- [75] Yamaguchi H, Tokura Y, Miyashita S and Hirayama Y 2004 Quantum interference effects in the magnetopiezoresistance of InAs/AlGaSb quasi-one-dimensional electron systems *Phys. Rev. Lett.* **93** 036603
- [76] Verbridge S S, Parpia J M, Reichenbach R B, Bellan L M and Craighead H G 2006 High quality factor resonance at room temperature with nanostrings under high tensile stress *J. Appl. Phys.* **99** 124304
- [77] Cole G D *et al* 2014 Tensile strained $\text{In}_x\text{Ga}_{1-x}\text{P}$ membranes for cavity optomechanics *Appl. Phys. Lett.* **104** 201908
- [78] He R, Feng X L, Roukes M L and Yang P 2008 Self-transducing silicon nanowire electromechanical systems at room temperature *Nano Lett.* **8** 1756–61
- [79] Gil-Santos E, Ramos D, Martinez J, Fernandez-Regulez M, Garcia R, San Paulo A, Calleja M and Tamayo J 2010 Nanomechanical mass sensing and stiffness spectrometry based on two-dimensional vibrations of resonant nanowires *Nature Nanotechnol.* **5** 641–5
- [80] Yeo I *et al* 2013 Strain-mediated coupling in a quantum dot-mechanical oscillator hybrid system *Nature Nanotechnol.* **9** 106–10
- [81] Gloppe A, Verlot P, Dupont-Ferrier E, Siria A, Poncharal P, Bachelier G, Vincent P and Arcizet O 2014 Bidimensional nano-optomechanics and topological backaction in a non-conservative radiation force field *Nature Nanotechnol.* **9** 920–6
- [82] Montinaro M, Wüst G, Munsch M, Fontana Y, Russo-Averchi E, Heiss M, Fontcuberta i Morral A, Warburton R J and Poggio M 2014 Quantum dot optomechanics in a fully self-assembled nanowire *Nano Lett.* **14** 4454
- [83] Sansa M, Fernández-Regulez M, Llobet J, Ivarro Paulo Á S and Pérez-Murano F 2014 High-sensitivity linear piezoresistive transduction for nanomechanical beam resonators *Nature Comm.* **4** 4313
- [84] Rossi N, Braakman F R, Cadeddu D, Vasyukov D, Tütüncüoğlu G, Fontcuberta i Morral A and Poggio M 2017 Vectorial scanning force microscopy using a nanowire sensor *Nature Nanotechnol.* **12** 150–5
- [85] de Lepinay L M, Pigeau B, Besga B, Vincent P, Poncharal P and Arcizet O 2017 A universal and ultrasensitive vectorial nanomechanical sensor for imaging 2D force fields *Nature Nanotechnol.* **12** 156–62
- [86] Bohm J and Farnell G W 1966 GaAs transducers *IEEE Trans. Sonic and Ultrasonics* **13** 125–9
- [87] Kline G R and Lakin K M 1983 1.0 GHz thin-film bulk acoustic wave resonators on GaAs *Appl. Phys. Lett.* **43** 750–1

- [88] Popa L C and Weinstein D 2013 Switchable piezoelectric transduction in AlGa_N/Ga_N MEMS resonators *Proc. 17th Int. conference on Solid-State Sens. Actuators Microsyst.* **2461–4**
- [89] Beck R, Eriksson M, Westervelt R M, Campman K L and Gossard A C 1996 Strain-sensing cryogenic field-effect transistor for integrated strain detection in GaAs/AlGaAs micro-electromechanical systems *Appl. Phys. Lett.* **68** 3763–5
- [90] Beck R G, Eriksson M A, Topinka M A, Westervelt R M, Maranowski K D and Gossard A C 1998 GaAs/AlGaAs self-sensing cantilevers for low temperature scanning probe microscopy *Appl. Phys. Lett.* **73** 1149–51
- [91] Oda Y, Onomitsu K, Kometani R, Warisawa S, Ishihara S and Yamaguchi H 2011 Electromechanical displacement detection with an on-chip high electron mobility transistor amplifier *Jpn. J. Appl. Phys.* **50** 06GJ01
- [92] Cleland A N, Aldridge J S, Driscoll D C and Gossard A C 2002 Nanomechanical displacement sensing using a quantum point contact *Appl. Phys. Lett.* **81** 1699–701
- [93] Knobel R G and Cleland A N 2003 Nanometre-scale displacement sensing using a single electron transistor *Nature* **424** 291–3
- [94] Poggio M, Jura M P, Degen C L, Topinka M A, Mamin H J, Goldhaber-Gordon D and Rugar D 2008 An off-board quantum point contact as a sensitive detector of cantilever motion *Nat. Phys.* **4** 635
- [95] Aspelmeyer M, Kippenberg T J and Marquard F 2014 *Cavity Optomechanics: Nano- and Micromechanical Resonators Interacting with Light* (Berlin: Springer)
- [96] Aspelmeyer M, Kippenberg T J and Marquard F 2014 Cavity optomechanics *Rev. Mod. Phys.* **86** 1391
- [97] Usami K, Naesby A, Bagci T, Melholt Nielsen B, Liu J, Stobbe S, Lodahl P and Polzik E S 2012 Optical cavity cooling of mechanical modes of a semiconductor nanomembrane *Nature Phys.* **8** 168–72
- [98] Favero I 2014 Gallium arsenide disks as optomechanical resonators *Cavity Optomechanics* (Berlin: Springer)
- [99] Gil-Santos E, Baker C, Nguyen D T, Lemaître A, Gomez C, Leo G, Ducci S and Favero I 2015 High frequency nano-optomechanical disk resonators in liquids *Nat. Nanotechnol.* **10** 810–6
- [100] Bergeal N, Schackert F, Metcalfe M, Vijay R, Manucharyan V E, Frunzio L, Prober D E, Schoelkopf R J, Girvin S M and Devoret M H 2010 Phase-preserving amplification near the quantum limit with a Josephson ring modulator *Nature* **465** 64
- [101] Matzuk T 1970 Mechanical parametric amplification *J. Acoust. Soc. America* **48** 21–6
- [102] Rugar D and Grütter P 1991 Mechanical parametric amplification and thermomechanical noise squeezing *Phys. Rev. Lett.* **67** 699–702
- [103] Turner K L, Miller S A, Hartwell P G, MacDonald N C, Strogatz S H and Adams S G 1998 Five parametric resonances in a microelectromechanical system *Nature* **396** 149–52
- [104] Carr D W, Evoy S, Sekaric L, Craighead H G and Parpia J M 2000 Parametric amplification in a torsional microresonator *Appl. Phys. Lett.* **77** 1545–7
- [105] Zhalutdinov M, Olkhovets A, Zehnder A, Ilic B, Czaplowski D, Craighead H G and Parpia J M 2001 Optically pumped parametric amplification for micromechanical oscillators *Appl. Phys. Lett.* **78** 3142–4
- [106] Unterreithmeier Q P, Weig E M and Kotthaus J P 2009 universal transduction scheme for nanomechanical systems based on dielectric forces *Nature* **458** 1001–4
- [107] Villanueva L G, Karabalin R B, Matheny M H, Kenig E, Cross M C and Roukes M L 2011 A Nanoscale parametric feedback oscillator *Nano Lett.* **11** 5054–9
- [108] Nayfeh A H and Mook D T 1995 *Nonlinear Oscillations* (Weinheim: Wiley-VCH Verlag GmbH & Co. KGaA) ch 5
- [109] Westra H J R, Poot M, van der Zant H S J and Venstra W J 2010 *Phys. Rev. Lett.* **105** 117205
- [110] Yamaguchi H and Mahboob I 2013 Parametric mode mixing in asymmetric doubly clamped beam resonators *New J. Phys.* **15** 015023
- [111] Mahboob I, Nishiguchi K, Okamoto H and Yamaguchi H 2012 Phonon-cavity electromechanics *Nature Phys.* **8** 387–92
- [112] Dunn T, Wenzler J-S and Mohanty P 2010 *Appl. Phys. Lett.* **97** 123109
- [113] Faust T, Rieger J, Seitner M J, Krenn P, Kotthaus J P and Weig E M 2012 Nonadiabatic dynamics of two strongly coupled nanomechanical resonator modes *Phys. Rev. Lett.* **109** 037205
- [114] Mahboob I, Flurin E, Nishiguchi K, Fujiwara A and Yamaguchi H 2010 Enhanced force sensitivity and noise squeezing in an electromechanical resonator coupled to a nanotransistor *Appl. Phys. Lett.* **97** 253105
- [115] Goto E 1959 The parametron, a digital computing element which utilises parametric oscillation *Proc. IRE* **47** 1304–16
- [116] Mahboob I, Mounaix M, Nishiguchi K, Fujiwara A and Yamaguchi H 2014 A multimode electromechanical parametric resonator array *Sci. Rep.* **4** 4448
- [117] Caves C M, Thorne K S, Drever R W P, Sandberg V D and Zimmermann M 1980 On the measurement of a weak classical force coupled to a quantum-mechanical oscillator: I. Issues of principle *Rev. Mod. Phys.* **52** 341
- [118] Bocko M F and Onofrio R 1996 On the measurement of a weak classical force coupled to a harmonic oscillator: experimental progress *Rev. Mod. Phys.* **68** 755–99
- [119] Palomaki T A, Teufel J D, Simmonds R W and Lehnert K W 2013 Entangling mechanical motion with microwave fields *Science* **342** 710–3
- [120] Wollman E E, Lei C U, Weinstein A J, Suh J, Kronwald A, Marquardt F, Clerk A A and Schwab K C 2015 Quantum squeezing of motion in a mechanical resonator *Science* **349** 952
- [121] Moreno-Moreno M, Ramana A, Gomez-Herrero J and Reifenberger R 2006 Parametric resonance based scanning probe microscopy *Appl. Phys. Lett.* **88** 193108
- [122] Gerry C C and Knight P L 2005 *Introductory Quantum Optics* (Cambridge: Cambridge University Press)
- [123] Mahboob I, Flurin E, Nishiguchi K, Fujiwara A and Yamaguchi H 2011 Interconnect-free parallel logic circuits in a single mechanical resonator *Nature Communications* **2** 198
- [124] Ekert A K and Knight P L 1989 Correlations and squeezing of two-mode oscillations *American J. Phys.* **57** 692
- [125] Schliesser A, Rivière R, Anetsberger G, Arcizet O and Kippenberg T J 2008 Resolved-sideband cooling of a micromechanical oscillator *Nature Phys.* **4** 415–9
- [126] Teufel J D, Donner T, Li D, Harlow J W, Allman M S, Cicak K, Sirois A J, Whittaker J D, Lehnert K W and Simmonds R W 2011 Sideband cooling of micromechanical motion to the quantum ground state *Nature* **475** 359–63
- [127] Chan J, Mayer Alegre T P, Safavi-Naeini A H, Hill J T, Krause A, Gröblacher S, Aspelmeyer M and Painter O 2011 Laser cooling of a nanomechanical oscillator into its quantum ground state *Nature* **478** 89–92
- [128] Martínez-Sala R, Sancho J, Sánchez J V, Gómez V and Llinares J 1995 Sound attenuation by sculpture *Nature* **378** 241
- [129] Mohammadi S, Eftekhari A A, Hunt W D and Adibi A 2009 High-Q micromechanical resonators in a two-dimensional phononic crystal slab *Appl. Phys. Lett.* **94** 051906
- [130] Maldovan M 2013 Sound and heat revolutions in phononics *Nature* **503** 209–17

- [131] Eichenfield M, Chan J, Camacho R M, Vahala K J and Painter O 2009 Optomechanical crystals *Nature* **462** 78–82
- [132] Mohammadi S and Adibi A 2011 On chip complex signal processing devices using coupled phononic crystal slab resonators and waveguides *AIP Adv.* **1** 041903
- [133] Otsuka P H *et al* 2013 Broadband evolution of phononic-crystal-waveguide eigenstates in real- and k-spaces *Sci. Rep.* **3** 3351
- [134] Hatanaka D, Mahboob I, Onomitsu K and Yamaguchi H 2013 A phonon transistor in an electromechanical resonator array *Appl. Phys. Lett.* **102** 213102
- [135] Hatanaka D, Mahboob I, Onomitsu K and Yamaguchi H 2014 Phonon waveguides for electromechanical circuits *Nat. Nanotechnol.* **9** 520
- [136] Hatanaka D, Dodel A, Mahboob I, Onomitsu K and Yamaguchi H 2015 Phonon propagation dynamics in band-engineered one-dimensional phononic crystal waveguides *New J. Phys.* **17** 113032
- [137] Balram K C, Davanço M I, Dong Song J and Srinivasan K 2016 Coherent coupling between radiofrequency, optical and acoustic waves in piezo-optomechanical circuits *Nat. Photon.* **10** 346–52
- [138] Eisenstein J P 1985 High-precision torsional magnetometer: application to two-dimensional electron systems *Appl. Phys. Lett.* **46** 695–6
- [139] Eisenstein J P, Stormer H L, Narayanamurti V V, Cho A Y, Gossard A C and Tu C W 1985 Density of states and de Haas-van Alphen effect in two-dimensional electron systems *Phys. Rev. Lett.* **55** 875–8
- [140] Templeton I M 1988 A high-sensitivity torsional magnetometer for two-dimensional electron systems *J. Appl. Phys.* **64** 3570–3
- [141] Pottsddag A, Shepherddag R, Herrenden-Harkerddag W G, Elliottddag M, Jonesddag C L, Usherddag A, Jones G A C, Ritchie D A, Linfield E H and Grimshaw M 1996 Magnetization studies of Landau level broadening in two-dimensional electron systems *J. Phys.: Condensed Matter* **8** 5189–207
- [142] Wieggers S A J, Specht M, Lévy L P, Simmons M Y, Ritchie D A, Cavanna A, Etienne B, Martinez G and Wyder P 1997 Magnetization and energy gaps of a high-mobility 2D electron gas in the quantum limit *Phys. Rev. Lett.* **79** 3238–41
- [143] Schwarz M P, Grundler D, Meinel I, Heyn Ch. and Heitmann D 2000 Micromechanical cantilever magnetometer with an integrated two-dimensional electron system *Appl. Phys. Lett.* **76** 3564–6
- [144] Harris J G E, Awschalom D D, Maranowski K D and Gossard A C 2000 Magnetization and dissipation measurements in the quantum Hall regime using an integrated micromechanical magnetometer *J. Appl. Phys.* **87** 5102–4
- [145] Ruhe N, Springborn J I, Heyn C, Wilde M A and Grundler D 2006 Simultaneous measurement of the de Haas-van Alphen and the Shubnikov-de Haas effect in a two-dimensional electron system *Phys. Rev.* **74** 235326
- [146] Wixforth A, Kotthaus J P and Weimann G 1986 Quantum oscillations in the surface-acoustic-wave attenuation caused by a two-dimensional electron system *Phys. Rev. Lett.* **56** 2104–6
- [147] Shevyrin A A, Pogosov A G, Budantsev M V, Bakarov A K, Toropov A I, Rodyakina E E and Shklyayev A A 2015 Actuation and transduction of resonant vibrations in GaAs/AlGaAs-based nanoelectromechanical systems containing two-dimensional electron gas *Appl. Phys. Lett.* **106** 183110
- [148] Shevyrin A A, Pogosov A G, Bakarov A K and Shklyayev A A 2016 Piezoelectric electromechanical coupling in nanomechanical resonators with a two-dimensional electron gas *Phys. Rev. Lett.* **117** 017702
- [149] Okamoto H, Akazaki T, Ueki M and Yamaguchi H 2005 Strongly enhanced sensitivity of piezoresistive cantilevers by utilizing the superconducting proximity effect *Jpn. J. Appl. Phys. Part 2—Lett. Express Lett.* **44** L893–5
- [150] Etaki S, Poot M, Mahboob I, Onomitsu K, Yamaguchi H and van der Zant H S 2008 Motion detection of a micromechanical resonator embedded in ad.c. SQUID *Nat. Phys.* **4** 785–8
- [151] Poot M, Etaki S, Mahboob I, Onomitsu K, Yamaguchi H, Blanter Y M and van der Zant H S J 2010 Tunable backaction of a dc SQUID on an integrated micromechanical resonator *Phys. Rev. Lett.* **105** 207203
- [152] LaHaye M D, Buu O, Camarota B and Schwab K C 2004 Approaching the quantum limit of a nanomechanical resonator *Science* **304** 74–7
- [153] Naik A, Buu O, LaHaye M D, Armour D, Clerk A A, Blencowe M P and Schwab K C 2006 Cooling a nanomechanical resonator with quantum back-action *Nature* **443** 193–6
- [154] Okuyama R, Eto M and Brandes T 2013 Optical phonon lasing in semiconductor double quantum dots *J. Phys. Soc. Jpn.* **82** 013704
- [155] Khaetskii A, Golovach V N, Hu X and Zutic I 2013 Proposal for a phonon laser utilizing quantum-dot spin states *Phys. Rev. Lett.* **111** 186601
- [156] Armour A D, Blencowe M P and Zhang Y 2004 Classical dynamics of a nanomechanical resonator coupled to a single-electron transistor *Phys. Rev. B* **69** 125313
- [157] Blencowe M P, Imbers J and Armour A D 2005 Dynamics of a nanomechanical resonator coupled to a superconducting single-electron transistor *New J. Phys.* **7** 236
- [158] Wilson-Rae I, Zoller P and Imamoglu A 2004 Laser cooling of a nanomechanical resonator mode to its quantum ground state *Phys. Rev. Lett.* **92** 075507
- [159] Shevchenko S N, Rubanov D G and Nori F 2015 Delayed-response quantum back action in nanoelectromechanical systems *Phys. Rev. B* **91** 165422
- [160] Nishiguchi K, Fujiwara A, Ono Y, Inokawa H and Takahashi Y 2006 Room-temperature-operating data processing circuit based on single-electron transfer and detection with metal-oxide-semiconductor field-effect transistor technology *Appl. Phys. Lett.* **88** 183101
- [161] Shim S-B, Imboden M and Mohanty P 2007 Synchronized oscillation in coupled nanomechanical oscillators *Science* **316** 95–9
- [162] Karabalin R B, Cross M C and Roukes M L 2009 Nonlinear dynamics and chaos in two coupled nanomechanical resonators *Phys. Rev. B* **79** 165309
- [163] Karabalin R B, Lifshitz R, Cross M C, Matheny M H, Masmanidis S C and Roukes M L 2011 Signal amplification by sensitive control of bifurcation topology *Phys. Rev. Lett.* **106** 094102